Mon. Not. R. Astron. Soc. **350,** 47–65 (2004) doi:10.1111/j.1365-2966.2004.07636.x

Cosmic reionization by stellar sources: population III stars

Aaron Sokasian,[1⋆] Naoki Yoshida,[1,2] Tom Abel,[3] Lars Hernquist[1] and Volker Springel[4]

[1]*Harvard-Smithsonian Center for Astrophysics, 60 Garden Street, Cambridge, MA 02138, USA*
[2]*National Astronomical Observatory of Japan, Mitaka, Tokyo 181-8588, Japan*
[3]*Department of Astronomy and Astrophysics, Penn State University, 525 Davey Lab, University Park, PA 16802, USA*
[4]*Max-Plank-Institut für Astrophysik, Karl-Schwarzschild-Straße, 1, 85740 Garching bei München, Germany*

Accepted 2004 January 16. Received 2004 January 15; in original form 2003 July 25

ABSTRACT

We combine fast radiative transfer calculations with high-resolution hydrodynamical simulations to study an epoch of early hydrogen reionization by primordial stellar sources at redshifts $15 \lesssim z \lesssim 30$. We consider the implications of various local and global feedback mechanisms using a set of models that bracket the severity of these effects to determine, qualitatively, how they may have influenced the global star formation rate and the details of hydrogen reionization. With relatively conservative assumptions, most of our models suggest that population III star formation proceeds in a self-regulated manner both locally and globally and, for a conventional ΛCDM cosmology, can significantly reionize the intergalactic medium between $15 \lesssim z \lesssim 20$ as long as a large fraction of ionizing photons can escape from these earliest galaxies.

We then combine these results with our earlier work focusing on the role of population II stars in galaxies with virial temperatures $\gtrsim 10^4$ K at redshifts $5 \lesssim z \lesssim 20$. Hence, we construct a complete reionization history of the Universe that matches the Thomson optical depths as measured by the *WMAP* satellite as well as the evolution of the Gunn–Peterson optical depth as seen in the absorption spectra of the highest redshift quasars. We find that even with conservative estimates for the impact of negative feedback mechanisms, primordial stellar sources contribute significantly to early reionization. Future observations of a Thomson optical depth of $\tau_e \gtrsim 0.13$ would bolster the claim for the existence of population III stars similar to the ones studied here.

Key words: radiative transfer – intergalactic medium – galaxies: starburst.

1 INTRODUCTION

The reionization history of the intergalactic medium (IGM) holds many important clues about the onset of structure formation and the nature of the first luminous sources. Advances made in the past few years are making it possible to probe this history directly. Spectroscopic observations of distant quasars by Fan et al. (2000) and Djorgovski et al. (2001) revealed that the IGM was highly ionized at $z \simeq 6$. Subsequent high-resolution studies of three $z > 5.8$ quasars by Becker et al. (2001) showed a significant increase in Lyα absorption from redshift 5.5 to 6.0 with the first possible detection of a Gunn–Peterson trough in the spectrum of the $z = 6.28$ quasar SDSS 1030.10+0524. More recently, White et al. (2003) presented an additional high-resolution spectrum of a quasar at $z = 6.37$ (Fan et al. 2003) which also appears to have an extended Gunn–Peterson trough. Together, these results indicate that the Universe was reionized only a short time earlier, implying a relatively late epoch for complete reionization.

Results from the *Wilkinson Microwave Anisotropy Probe* (*WMAP*) satellite (Kogut et al. 2003; Spergel et al. 2003) have challenged this scenario by suggesting that much of the IGM was ionized earlier than inferred from the SDSS quasars. In particular, the measured correlation between polarization and temperature yields an electron optical depth to the cosmmic microwave background (CMB) surface of last scattering of $\tau_e = 0.17$, corresponding to an instantaneous reionization epoch $z_r = 17$. The uncertainty associated with this measurement depends on fitting all parameters concerned with the TT power spectrum and the TE cross power spectrum. After a careful analysis, Kogut et al. (2003) have reported a 68 per cent confidence range of $0.13 < \tau_e < 0.21$ corresponding to an instantaneous reionization epoch $14 < z_r < 20$. In contrast, if reionization was completed around $z \sim 8$–10, as is suggested by the SDSS quasars, the electron optical depth would be only $\tau_e \sim 0.05$–0.06.

⋆E-mail: asokasia@cfa.harvard.edu

Although the discrepancy is only at the $\sim 3\sigma$ level, it is timely to explore the connection between the two sets of observations.

In a previous paper (Sokasian et al. 2003 hereafter Paper I), we used a high-resolution cosmological simulation in conjunction with a fast 3D radiative transfer code to study how stellar sources similar to those seen in local galaxies, i.e. population II type, contributed to the reionization history of the IGM in the redshift interval $6 \lesssim z \lesssim 20$. This work was similar to other related numerical studies (e.g. Gnedin 2000; Ciardi et al. 2000b; Razoumov et al. 2002; Ciardi, Stoehr & White 2003) except that source intensities were derived directly from intrinsic star formation rates computed in the underlying hydrodynamical simulations. In addition, the high mass resolution of the simulation allowed us to include sources down to $M \sim 4.0 \times 10^7 h^{-1}$ M$_\odot$ in a $10.0h^{-1}$ Mpc comoving box, which proved to have a significant impact on the reionization process. Our results showed that the star formation history inferred by Springel & Hernquist (2003) based on detailed hydrodynamic simulations and estimated analytically by Hernquist & Springel (2003) led to a relatively late reionization epoch near $z \simeq 7$–8 for a plausible range of escape fractions. Additionally, we generated synthetic spectra from a range of models with different escape fractions and showed that values in the range 10–20 per cent led to good statistical agreement with observational constraints on the neutral fraction of hydrogen at $z \sim 6$ derived from the $z = 6.28$ SDSS quasar of Becker et al. (2001). However, the relatively late reionization epoch predicted by these models cannot account for the high electron scattering optical depth inferred from the *WMAP* measurements.

In an effort to study how this difference could be reconciled, we employed heuristic models with an evolving ionizing boosting factor and found that in order to simultaneously match the *WMAP* and SDSS constraints, one requires an $f_{\rm esc} = 0.20$ model with a boosting factor that rises from unity at $z \simeq 6$ to $\gtrsim 50$ near $z \sim 18$. In this picture, large boosting factors mean that the stellar production rate of ionizing photons is much higher than that which would be produced according to our model assumptions. One mechanism that would boost the production rate of ionizing photons would be if the stellar IMF evolved so that it became increasingly top-heavy at high redshift. While possible, this scenario would still result in an IGM that is highly ionized at $z < 13$, a condition which may be inconsistent with the thermal history of the IGM. More specifically, (see also Theuns et al. 2002) have shown that as long as the Universe is reionized before $z = 10$ and remains ionized thereafter, the IGM would reach an asymptotic thermal state that is too cold in comparison with the temperature inferred from Lyα forest observations at $z \sim 2$–4. This conclusion, however, relies on assumptions regarding the ionizing spectrum. For example, if the ionizing spectrum is harder than the typical quasar spectrum above the H I and He I ionization thresholds, then order unity changes in the ionization fraction of H I and He I are necessary in the range $6 < z < 10$ in order to sufficiently heat up the IGM within the observation constraint at $z \approx 4$. However, if the spectrum is relatively soft (more typical of population II stars) then this condition is avoided as long as He II reionization occurs relatively late near $z \sim 4$ (see, for example, Sokasian, Abel & Hernquist, 2002).

Another difficulty with boosting the production rate of ionizing photons, as emphasized by e.g. Yoshida et al. (2003a); Yoshida,Bromm & Hernquist (2003e), is that the IMF would need to remain top heavy for many generations of high-mass stars. These stars have typical lifetimes $\sim$ a few million years. However, the total elapsed time between $z = 18$ and $z = 10$ is more than a hundred times longer; therefore, it would be necessary for massive star formation to proceed efficiently for more than 100 generations. Studies by e.g. Omukai (2000), Bromm et al. (2001a), and Schneider et al. (2002) indicate that very massive stars can form only if the metallicity of the gas lies below a critical threshold, $Z \lesssim 10^{-3.5} Z_\odot$. It appears problematic for the gas in star-forming haloes to remain sufficiently chemically pristine for massive star formation to continue for over 100 stellar generations.

The combined observational constraints summarized above suggest that the reionization history of the Universe was complex, perhaps having had multiple reionization epochs. Such a scenario has been considered by Cen (2003b) and Wyithe & Loeb (2003b), who pointed out the possibility that the Universe was first reionized by an early generation of massive, metal-free (population III) stars, but that then much of the IGM recombined once these stars were no longer able to form, and the Universe was subsequently reionized a second time by the next generation of population II stars. In hierarchical models of structure formation, these 'first (metal-free) stars' are thought to form through molecular hydrogen (H_2) cooling in haloes with masses larger than $\sim 7 \times 10^5$ M$_\odot$ at redshifts as high as $z \sim 20$–30, provided that the haloes are dynamically cold and contain sufficiently larger numbers of hydrogen molecules (Yoshida et al. 2003c).

Recent progress in simulating the formation of the very first objects in the Universe (Abel et al. 1998; Bromm, Coppi & Larson 1999) has shown that the first luminous objects to form in CDM models are stars. In addition, because the first H II regions are capable of driving out most of the gas from the halo, it is unlikely that massive seed black holes are able to accrete within a Hubble time after they formed (Whalen, Abel & Norman 2003). The notion that these population III stars played a role in cosmological reionization in cold dark matter (CDM) models has been discussed widely (e.g. Couchman & Rees 1986; Barkana & Loeb 2001;Mackey, Bromm & Herquinst 2003; Venkatesan, Tumlinson & Shull 2003; Cen 2003a; Wyithe & Loeb 2003a; Yoshida et al. 2003a,b). Simulations indicate that these stars which form in 'mini-haloes' should be massive $\gtrsim 100$ M$_\odot$ (Abel, Bryan & Norman 2000; Abel, Bryan & Norman 2002; Bromm, Coppi & Larson 2002). Whereas Abel et al. (2002) predict one massive star per halo Bromm et al. (2002) suggest that multiple stars can be produced in each dark matter halo. We discuss both scenarios in this paper. Such population III stars are efficient UV emitters because of their approximately constant effective surface temperatures near 10^5 K with lifetimes of $\sim 3 \times 10^6$ yr, independent of their mass (e.g. Bromm, Kudritzki & Loeb 2001b; Schaerer 2002 for recent discussions). In fact, these stars are capable of producing up to $\sim$30 times more ionizing photons per baryon compared with population II stars with a Salpeter IMF.

Although the impressive yield of ionizing photons from population III stars appears promising in terms of a possible solution to the early reionization epoch suggested by *WMAP*, there are still many questions remaining as to whether enough of these first generation stars could have formed to cause cosmic reionization. In general, semi-analytic modelling has been used to address these questions (see, e.g. Wyithe & Loeb 2003a,b; Cen 2003a,b); however, the predictions of these models are often uncertain because of the relatively crude assumptions used to relate luminous objects to the dark matter haloes which host them. For example, Yoshida et al. (2003c) have shown that simple criteria based on only the mass or virial temperatures of haloes can fail by an order of magnitude or more because of dynamical heating by mergers. Additionally, the effects of feedback processes are very difficult to assess in semi-analytic models. The UV radiation in the Lyman–Werner (LW) band (11.26–13.6 eV) from these massive stars can photodissociate the fragile H_2 molecules that are responsible for their formation. This negative

feedback can significantly limit population III star formation and thereby substantially reduce the effective ionizing flux in the early Universe. Conversely, it has been argued that feedback from X-rays can promote H_2 production by boosting the free electron fraction in distant regions (Haiman, Rees & Loeb 1996; Oh 2001). Efforts to explore feedback effects on cooling and collapsing gas have been pursued by many groups (e.g. Dekel & Rees 1987; Haiman, Rees & Loeb 1997; Haiman, Abel & Rees 2000). However, these studies have primarily relied on semi-analytic methods, which assume spherically symmetry and ignore details regarding formation dynamics and locations of haloes in complex density fields.

A more realistic analysis of the problem requires detailed numerical simulations capable of capturing the physics of early structure formation and related feedback effects. This was first attempted by (see also Machacek, Bryan & Abel 2003 Machacek, Bryan & Abel 2001 see also Machacek, Bryan & Abel 2003) who employed an Eulerian adaptive mesh refinement simulation to investigate the quantitative effects of a background radiation field on the subsequent cooling and collapse of high-redshift pre-galactic clouds. Ricotti, Gnedin & Shull (2002a); Ricotti, Gnedin & Shull (2002b) followed up on the numerical approach by including radiative transfer effects and found that the formation of small halo objects is not significantly suppressed by the dissociating background. More recently, Yoshida et al. (2003c) used high-resolution cosmological simulations which included a careful treatment of the physics of chemically pristine gas and the impact of a dissociating UV background to study the statistical properties of primordial haloes in cosmological volumes. In a subsequent study, Yoshida et al. (2003b) coupled radiative transfer calculations to their analysis to investigate reionization by an early generation of stars. More specifically, they identified plausible sites of star formation in their cosmological volume where they then placed massive stars with $M = 300$ M$_\odot$ under the usual 'one star per halo' assumption. They ran the multisource radiative transfer code described in Paper I on a 200^3 grid with the assumption that source lifetimes are 3 million years and that the escape fraction for ionizing radiation from the haloes is unity. To mimic the strong radiative feedback in H II regions, they implemented a 'volume exclusion effect' which disabled sources within already ionized regions. The results from their analysis indicated that in the standard ΛCDM cosmology, a sufficient number of population III sources turn on to reionize the volume fully by $z \simeq 18$. By merging the subsequent ionization history from population II sources (adopted from Paper I), they were able to compute a total optical depth to Thomson scattering of $\tau_e \sim 0.14$, in reasonable agreement with the *WMAP* result.

Encouraged by the results from Yoshida et al.(2003b), the aim of this paper is to use the numerical approach outlined in Paper I to perform a more rigorous study of the parameter space associated with the ability of population III stars to reionize the Universe. In particular, by tracking individual clouds of dense molecular gas directly, we are able to implement simulated feedback effects explicitly. We explore a number of plausible models in which we incorporate feedback effects in an ad hoc fashion and examine the corresponding ionization history of the Universe. By coupling this history with the results from the population II analysis conducted in Paper I, we are able to assess the overall success of each model in terms of the *WMAP* and SDSS observations.

This paper is organized in the following manner. In Section 2 we describe the cosmological simulation used in our analysis. Then in Section 3 we describe our methodology for source selection and present a detailed discussion of how we approximate related feedback effects. The results of the simulation are presented in Section 4. Included in this section is a discussion related to the reionization history of the Universe from the combined effect of population II and population III stars. Finally in Section 5, we provide a summary and state our conclusions.

2 UNDERLYING COSMOLOGICAL SIMULATION

The underlying simulation used in this paper was performed using the parallel Tree-PM/SPH solver GADGET2, in its fully conservative entropy form (see Springel & Hernquist 2002). The simulation follows the non-equilibrium reactions of nine chemical species (e^-, H, H^+, He, He^+, He^{++}, H_2, $H^+{}_2$, H^-) using the reaction coefficients compiled by Abel et al. (1997). The cooling rate of Galli & Palla (1998) is employed for molecular hydrogen. In this paper, we will focus on a ΛCDM model with matter density $\Omega_m = 0.3$, baryon density $\Omega_b = 0.04$, cosmological constant $\Omega_\Lambda = 0.7$ and expansion rate at the present time $H_0 = 70$ km s^{-1} Mpc^{-1}. The spectral index of the primordial power spectrum has been set to $n_s = 1$ and we normalize the fluctuation amplitude by setting $\sigma_8 = 0.9$. Further details of the simulation and methods for generating initial conditions are given in Yoshida et al. (2003c) and Yoshida, Sugiyama & Hernquist (2003d), respectively.

The particular simulation we use employs 2×324^3 particles in a cosmological volume of 1 Mpc on a side, corresponding to a mass resolution of 160 M$_\odot$ and 1040 M$_\odot$ for gas and dark matter particles, respectively. Convergence tests using higher resolution simulations indicate that the mass resolution adopted here is sufficient to follow the cooling and collapse of primordial gas within low-mass ($\sim 10^6$ M$_\odot$) haloes.

Owing to the relatively small size of our simulation box, the fundamental fluctuation mode starts to become non-linear at $z \approx 16$, forcing us to stop our analysis at this redshift. We discuss the limitations of such a small volume in the context of predicting cosmic reionization in Section 4.

3 SOURCE DEFINITION AND FEEDBACK EFFECTS

3.1 Source definition

Our approach for defining sources relies on identifying virialized haloes, which contain a reservoir of cold and dense gas that undergoes star formation. This requires first locating dark matter haloes via a friends-of-friends (FOF) algorithm with a linking parameter $b = 0.164$ in units of mean particle separation, and discarding groups with fewer than 100 dark matter particles. For each FOF group, we compute a virial radius R_{vir} defined as the radius of the sphere centred on the most bound particle of the group having an overdensity of 180 relative to the critical density. Within this radius we then measure the mass of gas that is cold ($T < 500$ K) and dense ($n_H > 500$ cm^{-3}). The clouds of molecular gas in these reservoirs are expected to cool rapidly and exceed the characteristic Jeans mass $M_J \sim 3000$ M$_\odot$ for the typical temperature $T \sim 200$ K and density $n_H \sim 10^3$ cm^{-3} of the condensed gas. The haloes which contain these reservoirs of cold gas are therefore considered to be sites of active star formation and serve as potential locations for population III sources. In the top panel of Fig. 1 we show how cold gas accumulates in star-forming haloes as a function of redshift. Here, star-forming haloes (*solid circles*) are plotted at each simulation snapshot (separated in time by 3×10^6 yr) and serve to illustrate how cold gas accumulates within individual haloes over time. In the

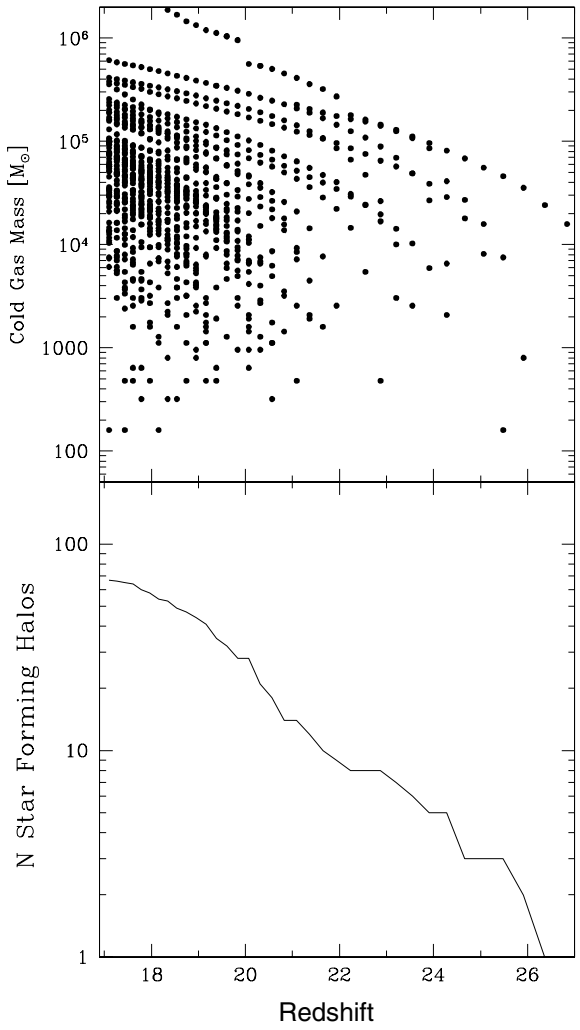

Figure 1. Top panel: the amount of cold gas ($T < 500$ K and $n_{\rm H} > 500$ cm^{-3}) in star-forming haloes as a function of redshift. Star-forming haloes are plotted at each simulation snapshot (separated in time by 3×10^6 yr). Bottom panel: the total number of star forming haloes in our simulation volume as a function of redshift.

bottom panel of the same figure we show the total number of star forming haloes as function of redshift in our simulation volume. It is important to point out that in carrying out our analysis, we construct a halo merger history and use it to carefully track the star-forming gas that is exchanged between the progenitors and descendants of each halo.

For each potential source site, we compute the amount of gas that actually forms stars by multiplying the total amount of cold gas in the halo by the free parameter $E_{\rm SF}$. Here $E_{\rm SF}$ can be thought of as a universal star formation efficiency of *dense cold* gas as defined above to form sources and should not be confused with similar definitions of star formation efficiencies based on the *total* amount of gas in the halo (see, e.g. Cen 2003a,b). In this study, we consider two different values for this parameter: $E_{\rm SF} = 0.02$, and $E_{\rm SF} = 0.005$. For a given value of $E_{\rm SF}$, we apply a further restriction on the allowable mass of stars $M_\star$ that can actually form. More specifically, we assume that the primordial IMF is moderately top-heavy and yields stars with masses in the range 100–300 $M_\odot$. We therefore first discard all haloes with star masses below 100 $M_\odot$. Above this limit, we allow a range of star masses to be incorporated into the halo up to a maximum of 900 $M_\odot$ under the assumption that only a few stars can form at coincidentally close times and thus survive the intense dissociating radiation from the first star in the halo (see Omukai & Nishi 1999; Abel et al. 2002) and its subsequent explosion (e.g. Bromm, Yoshida & Hernquist 2003). Our assumption may therefore be considered as a slightly more relaxed version of the 'one-star-per-halo' prescription employed in related studies of this topic (see, e.g. Oh et al. 2001b). Nevertheless, it should be noted that the associated parameter space which will be explored in this study leads to relatively few multi-source haloes ($M_\star > 300$ $M_\odot$) under the assumption of a moderately top-heavy IMF and therefore leads to similar results.

Because of their high mass, population III stars are dominated by radiation pressure and have luminosities close to the Eddington limit $L_{\rm Edd}$. This leads to a constant source lifetime estimated to be $t \simeq 0.007Mc^2/L_{\rm Edd} \sim 3 \times 10^6$ yr. We use this value as the universal lifetime for all our stars and also adopt it as the time-step over which we evolve our simulation. To compute ionizing intensities we first note the results presented in Bromm et al. (2001a), who demonstrated that population III stars with masses $\geqslant$300 $M_\odot$ have a generic mass-scaled spectral form that is almost independent of mass resulting in H I and He II ionizing photon production rates 1.6×10^{48} s^{-1} $M^{-1}_\odot$ and 3.8×10^{47} s^{-1} $M^{-1}_\odot$, respectively. For 100 $M_\odot$ stars, the number of ionizing photons per solar mass is reduced by a factor of $\sim$2 for H I and $\sim$4 for He II (Bromm et al. 2001a; Tumlinson & Shull 2000). Given our assumption of the 100–300 $M_\odot$ mass range for individual stars, we compute ionization rates for haloes by interpolating between the values quoted above for the 100-$M_\odot$ and $\geqslant 300 - M_\odot$ cases.[1] In the relatively few haloes where the total source mass exceeds 300 $M_\odot$, we adopt the median values of 1.2×10^{48} s^{-1}M$^{-1}_\odot$ for H I and 2.4×10^{47} s^{-1}M$^{-1}_\odot$ for He II under the assumption that these haloes contain multiple stars with masses in the range 100–300 $M_\odot$.

The quantity of ionizing flux that can actually escape a halo and enter into the IGM is parameterized by the escape fraction $f_{\rm esc}$. In this context, $f_{\rm esc}$ is defined to be the fraction of ionizing photons intrinsic to each source that escape the virial radius of the halo and participate in the radiative transfer calculations. It must be noted here that this parameter inevitably also carries with it any uncertainties associated with the shape of the galaxy, the gas and stellar density profiles, and the IMF and star formation efficiency. At low redshifts, observations deduced from $z < 3$ starburst galaxies (see Heckman et al. 2001; Hurwitz, Jenlinsky & Dixon 1997; Leitherer et al. 1995) suggest small values for $f_{\rm esc}$ around $f_{\rm esc} \lesssim 0.10$. However, it is important to note that these observational results may be underestimating the true values owing to undetected absorption from interstellar components. In fact, observations of 29 Lyman break galaxies at $z \sim 3.4$ by Steidel, Pettini & Adelberger (2001) appear to suggest much larger escape fractions. Furthermore, it is unclear how the relevant factors associated with the escape fraction vary with redshift. Theoretical work on $f_{\rm esc}$ at high redshifts (Wood & Loeb 2000; Ricotti & Shull 2000) finds small values, although these estimates are highly uncertain owing to the lack of information regarding the IMF and star formation efficiencies at early times. In addition, the effect of

[1] Note that in our simulations we carry out radiative transfer calculations to track H II and He III regions only, with the implicit assumption that for massive stars, the boundaries of the ionization zones for He II and H II coincide. This serves to significantly speed up our calculations by allowing the tracking of both zones via a single ray tracing calculation in H II; see Section 2.1 of Paper I for further details.

dust, complex gas inhomogeneity and gas dynamics, all of which may strongly influence escape fractions, are not included in these theoretical studies. More recently, Whalen et al. (2003) have studied the ionization environment of the first luminous objects using detailed one-dimensional radiation hydrodynamical simulations and find that the transition from D to R-type fronts occurs within only ∼100 000 yr after the star reaches the zero-age main sequence. Because these I-fronts exit the halo on time-scales much shorter that the main sequence lifetime of the stars, their host haloes can have UV escape fractions of $\gtrsim$0.95.

Given these recent results, we employ relatively large escape fractions, $f_{\rm esc} = 1$ and $f_{\rm esc} = 0.3$, in all the models we consider. The escape fraction of unity is motivated by the extreme cases from Whalen et al. (2003) while the escape fraction of 0.3 is meant to represent an alternate case where the surrounding environment is much more complex and restrictive to ionizing breakthroughs.

3.2 Feedback effects

Feedback effects from the first stars inevitably exert prompt and significant impact on subsequent star formation. Locally, population III stars are expected to significantly affect their environments when they explode as supernovae (e.g. Bromm et al. 2003). This 'internal' feedback will perturb the gas and effectively regulate subsequent star formation in the pregalactic cloud. Feedback from the first stars can also affect structure formation on a global scale. This is because the UV photons below 13.6 eV produced by these stars can easily propagate through the Universe and build up a soft UV background that can alter the chemistry of distant regions. More specifically, studies have suggested that even a feeble UV background can photodissociate the fragile H_2 molecules necessary for cooling of the primordial gas (see, e.g. Haiman, Rees & Loeb 1997; Haiman, Abel & Rees 2000; Ciardi, Ferrara & Abel 2000a; Machacek, Bryan & Abel 2001). Conversely, it has been argued that feedback may actually enhance H_2 formation ahead of of the ionization front (Ricotti, Gnedin & Shull 2001) or through the boosting of the electron fraction in dense regions by X-rays emitted from, for example, distant supernovae remnants (Haiman et al. (1996); Cen 2003a ; but see also Machacek, Bryan & Abel 2003, who find that the net effect of X-rays is rather mild).

Presently, the technical difficulties involved with the incorporation of radiative transfer calculations directly into cosmological simulations prevent us from studying these effects numerically in a fully consistent manner. We therefore adopt a more ad hoc approach which attempts to include feedback effects through the incorporation of simple, physically motivated criteria which dynamically constrain the amount of stellar mass that forms. In the following two sections we will describe our prescription for parameterizing internal and external feedback effects within the context of our simulation.

3.2.1 Simulating internal feedback effects

Stars with masses in the range $140\,{\rm M}_\odot \lesssim M \lesssim 260\,{\rm M}_\odot$ are expected to die as supernovae which release up to 10^{53} erg of kinetic energy into their surroundings (e.g. Heger & Woosley 2002). Since the gravitational binding energy for gas in sub-galactic haloes is $E_{\rm b} \sim 10^{49}[M/(5 \times 10^5)]^{5/3}[(1+z)/20]$, these explosions can severely disrupt their immediate surroundings, possibly *driving away* a large portion of the gas from the halo (see e.g. Bromm et al. 2003). To mimic this effect, we introduce an 'internal disruption factor' $D_{\rm f}$ which will parametrize the amount of gas that gets blown out. More specifically, for every halo which turns on with star mass $M_\star$, we flag a corresponding amount of star-forming gas mass $M_{\rm SF}$ (cold gas) equivalent to $D_{\rm f} \times M_\star$ within that halo as unusable for future star formation. The prescription for calculating a new star mass for a given halo is then quantified at each time-step i in terms of $E_{\rm SF}$ by the expression

$$M_\star^i = E_{\rm SF}\left[M_{\rm SF}^{i-1}(1 - E_{\rm SF}D_{\rm f}) + \Delta M_{\rm SF}^i\right], \quad (1)$$

where $M_{\rm SF}^{i-1}$ represents the amount of *usable* star-forming gas mass from the previous step and $\Delta M^i{}_{\rm SF}$ is the amount of new star-forming gas accumulating in the halo at the current step. This prescription requires us to track explicitly and directly the history of gas in each halo, accounting for the accumulation of new star-forming gas by continuing accretion from surrounding gas, and also from mergers with other star-forming haloes. In this analysis, we explore a case where the disruption factor is small, $D_{\rm f} = 40$, and also a case where the disruption factor is large, $D_{\rm f} = 120$. We admit that these choices for the disruption factor are somewhat arbitrary. However, our aim here is to use $D_{\rm f}$ in conjunction with $E_{\rm SF}$ to create a range of different models which span the plausible parameter space associated with internal feedback effects. In particular, our choice of $D_{\rm f} = 40$ will describe a scenario where clumps of condensed gas in the halo only inefficiently absorb the energy released from a local supernova (possibly owing to a spatially clustered distribution with a small cross-section and large column density to the explosion site) and are therefore marginally disrupted ($E_{\rm SF} \times D_{\rm f} = 0.2$–$0.8$). Such a low disruption factor may also be motivated by the potential positive feedback that can arise from propagating compression shocks induced by the exploding star, which may accelerate star formation within the halo (Mackey, Bromm & Hernquist 2003; Salvaterra, Ferrara & Schneider 2003). On the other hand, our choice of $D_{\rm f} = 120$ will simulate the case where energy absorption is efficient and effectively disperses a large amount ($E_{\rm SF} \times D_{\rm f} = 0.6$–$2.4$) of the gas. Here, values for $E_{\rm SF} \times D_{\rm f}$ close to unity correspond to the total disruption of star-forming gas within the halo, while values larger than unity are meant to represent an extreme disruption of the gas extending beyond the halo. Formally, the latter scenario results in negative star masses for some of the haloes immediately after a star-forming episode. In these cases we simply set the star mass to zero, but continue to track the amount of *negative* star-forming gas mass in the halo, which decreases in time as new gas is accumulated. Negative star-forming gas, in this context, represents a ramification of strong internal feedback effects which not only disrupt the available star-forming gas in the halo but also inhibit the future accretion of neighbouring gas surrounding the halo. In all cases, it is important to keep in mind that our parametrization of the disruption factor $D_{\rm f}$ also carries with it the uncertainty associated with whether or not the stars formed actually end their lives as supernovae.

In Fig. 2, we plot all the possible star-forming haloes in our simulation volume for the four different combinations of $D_{\rm f}$ and $E_{\rm SF}$ we tried. Here, the two dotted horizontal lines delineate the range of allowable star masses in haloes (*solid circles*) as described earlier. In particular, haloes with source masses falling short of 100 $M_\odot$ (*crosses*) are excluded while those above the 900 $M_\odot$ limit (*open circles*) are included, but with star masses artificially set to the upper limit of 900 $M_\odot$. A comparison between this figure and the top panel in Fig. 1 clearly demonstrates the effect of including a disruption mechanism in the haloes. Namely, once haloes acquire enough star mass to turn on, the surrounding star forming mass in that halo is disrupted to varying degrees and does not monotonically increase as a function of time. Consequently, a halo that has turned on at a

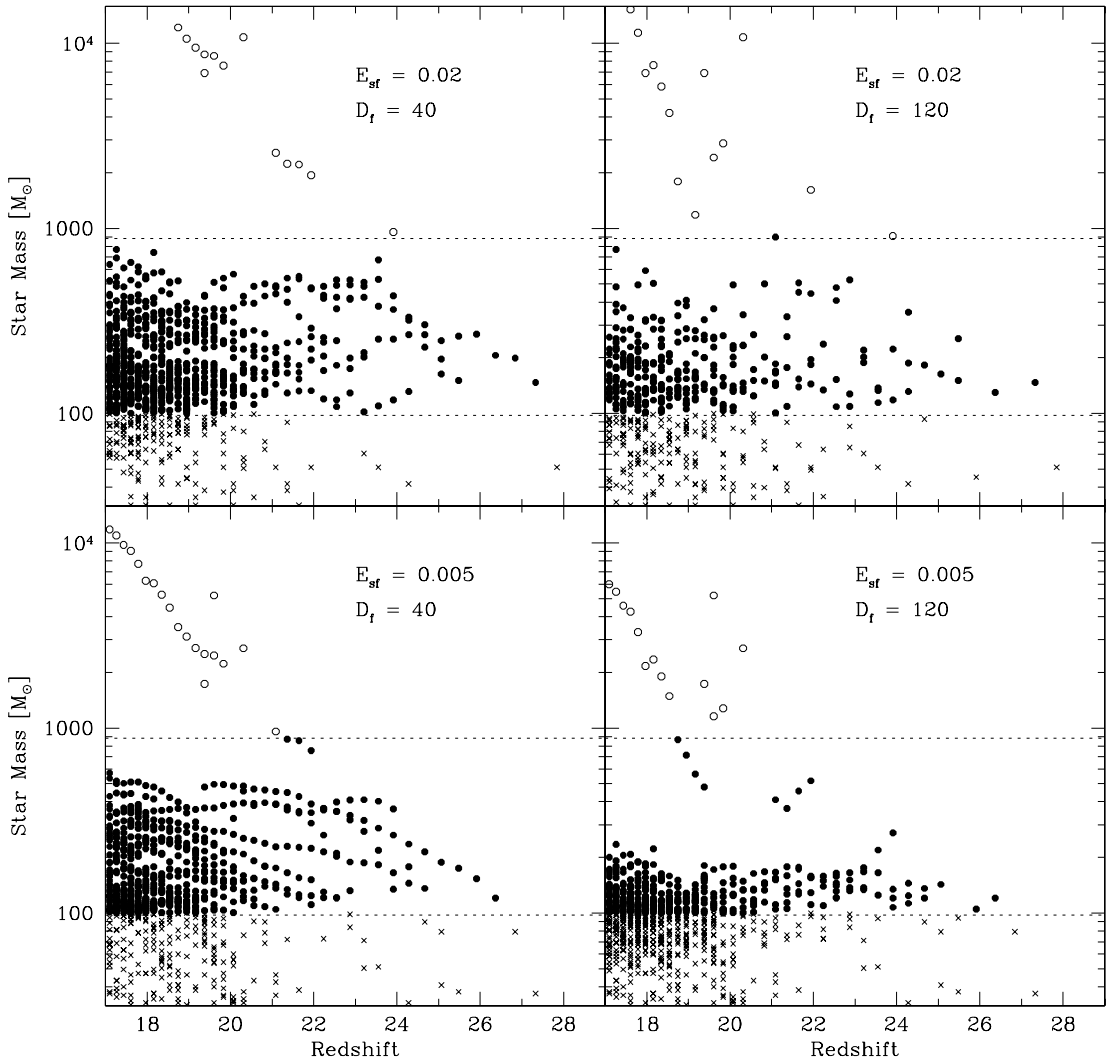

Figure 2. Total star masses in haloes as a function of redshift for different values of the disruption factor $D_{\rm f}$ and star formation efficiency $E_{\rm SF}$ (see text for discussion). Horizontal dotted lines indicate the range of allowed star masses in haloes (*solid circles*). Source masses falling below 100 $M_\odot$ mass (*crosses*) are excluded, while those above 900 $M_\odot$ (*open circles*) have star masses artificially set to an upper limit of 900 $M_\odot$.

given time may not have enough undisrupted star-forming gas at subsequent time-steps to turn on again. This effect is especially noticeable in the right-hand column where the disruption factor is high with the most dramatic case indicated in the top right panel. Here, the combination with a high efficiency factor renders most haloes incapable of turning on more than once. In the left-hand column, the disruption factor is three times smaller and most haloes are capable of turning on repeatedly. This is especially true in the bottom left panel where the efficiency is also small and individual haloes can be seen switching on continuously once they surpass the minimum star mass threshold. Interestingly, in all cases the most massive halo in our simulation volume appears to contain enough star-forming mass at redshifts below 20 that the disruption caused by a star mass of 900 $M_\odot$ switching on at each step does not inhibit subsequent star formation. This seems like a plausible scenario for haloes with very deep potential wells that are especially conducive to star formation. It must be noted that at some level there exists a degeneracy between the effects produced by the parameters $D_{\rm f}$ and $E_{\rm SF}$. However, as Fig. 2 demonstrates, there are distinct differences between the two parameters in terms of simulating the physical consequences of star formation, especially in extreme cases. We therefore continue our analysis with this distinction.

3.2.2 Simulating external feedback effects

We now turn to the issue of simulating external feedback effects that have a more global impact. The first type of external feedback we consider is related to the 'sphere of influence' associated with the ionization zone surrounding a source. The gas within this region is expected to be substantially photoheated to temperatures in excess of 2×10^4 K when ionized by radiation with a spectrum typical of metal-free stars (see Hui & Haiman 2003). For example, a 7×10^5 $M_\odot$ halo at $z \simeq 20$ has a binding energy of roughly $\sim 10^{49}$ erg, which is considerably less that the total ionizing energy produced by a single massive star of order $\sim 1 \times 10^{54} (M_{\rm star}/200\,M_\odot)$ erg. As a result, star-forming gas in shallow potential wells located within these ionized regions photo-evaporates and fails to produce stars. The magnitude of the effect is difficult to gauge without a self consistent treatment of radiative photo-heating effects linked directly

to the hydrodynamics of the gas. Since the radiative transfer and gas dynamics are not coupled in our calculations, we can only simulate the effect in an ad hoc manner. In particular, we would like to qualitatively mimic the inhibiting effects that photo-heating may have on star formation in haloes as function of the depth of their potential wells, or masses, as seen in the simulations of e.g. Bromm et al. (2003) and Whalen et al. (2003). For this, we implement an 'ionization exclusion effect' which will act to inhibit sources from turning on before a certain amount of time has passed since their gas was ionized. We express the recuperation time $t_{\rm recup}$ in terms of the free-fall time associated with each source cell. In a spherical potential, the free-fall time can be expressed as

$$t_{\rm ff} = \sqrt{\frac{3\pi}{32G\rho}}, \tag{2}$$

where G is the gravitational constant and ρ is the density. We note that free-fall times are calculated only for the overdense cells which actually contain sources, otherwise this time-scale is not meaningful. As a first order approximation, we use this expression to compute free-fall times in source cells according to their matter densities. We can then express the recuperation time in terms of the free-fall time $t_{\rm recup} = K_{\rm recup} t_{\rm ff}$. Here the free parameter $K_{\rm recup}$ can be thought of as the relative fraction of a free-fall time that must pass before a source halo can recuperate from the negative effects of photo-evaporation. This method requires us to track carefully when source cells become ionized (either by their own radiation or by the radiation of neighbouring sources) and subsequently increment the amount of time that passes in these cells at each time-step. It should be noted that we also track the migration of sources into different source cells during the course of a particular exclusion interval so as to properly follow the total wait time associated with each source halo. Owing to the large overdensities in source cells, recombination times are short and, as a result, it is possible for a given source cell to undergo multiple ionizations and inhibited phases. On a general level, this effect is very similar to the 'volume exclusion effect' adopted by Yoshida et al. (2003b) although our method has the convenient feature of naturally gauging the resiliency of each halo to be able to recuperate from photo-heating. To explore both a weak and strong case of this effect, we consider recuperation parameters $K_{\rm recup} = 1/3$ and $K_{\rm recup} = 2/3$.

Next, we turn to photodissociation of molecular hydrogen by the LW radiation from the first stars. While photons with energies above 13.6 eV are likely to be completely absorbed by the gas surrounding the sources, those with energies in the LW bands can easily travel unimpeded through the neutral IGM and build up a uniform UV background radiation field (Dekel & Rees 1987; Haiman et al. 2000; Omukai & Nishi 1999). We emphasize that the net effect of this radiation is *not* to completely inhibit primordial gas cooling, but it raises the minimum mass scale of the haloes in which the gas can cool (Haiman et al. 2000; Machacek et al. 2001). Recently, Yoshida et al. (2003c) studied the effect of LW backgrounds on the formation of primordial gas clouds and found that owing to the photodissociation of H_2, gas cooling is suppressed for radiation with intensity $J_{21} > 0.01$ (in units of 10^{21} erg s^{-1} cm^{-2} Hz^{-1} str^{-1}). They also implemented a technique to compute H_2 column densities around virialized regions making it possible to estimate gas self-shielding factors in their maximal limits. With the help of self-shielding, primordial gas in large haloes can cool efficiently even when exposed to background radiation with intensity $J_{21} = 0.01$. While the two extreme cases studied by Yoshida et al. (2003c), an optically thin limit and maximal gas self-shielding, should bracket the true effect of the LW background, a more careful study is required to obtain an accurate estimate of the impact of this radiation.

Given the uncertainties, we continue with our approach of adopting a simple parametrization aimed at capturing the qualitative aspects of the effect. In particular, we first note that LW radiation is only capable of affecting the abundance of molecular hydrogen in gas and does not significantly affect the thermal state of the gas. Assuming equilibrium, the amount of molecular hydrogen in a gas cloud is inversely proportional to the photodissociation reaction coefficient given by

$$k_{\rm diss} = 1.38 \times 10^9 J_{\rm LW} K_{\rm shield}, \tag{3}$$

where $J_{\rm LW}$ is the radiation intensity at $h\nu = 12.87$ eV and $K_{\rm shield}$ is the effective shielding factor. Neglecting the evolution of the gas density and temperature, and noting that the cooling rate scales just as the number of hydrogen molecules, the amount of gas that can cool should be proportional to $1/(J_{\rm LW} K_{\rm shield})$. Given this linear scaling we introduce a modulating function,

$$F_{\rm LW} = a(J_{\rm LW} K_{\rm shield} - x_0) + b, \tag{4}$$

from which the amount of cold gas available for star mass production is computed after the effects of photodissociation are taken into account. To determine the fitting parameters a, b and x_0, we refer to Yoshida et al. (2003c) who point out that LW radiation is unimportant for $J_{\rm LW} < 10^{-24}$, whereas for $J_{\rm LW} > 10^{-21}$ the gas cannot cool by molecular hydrogen cooling in nearly all the haloes in the optically thin limit ($K_{\rm shielding} = 1$). Thus by setting $a = 10^{21}$, $b = 1$, $x_0 = 10^{-24}$ and restricting the maximum value of $F_{\rm LW}$ to 1, we are able to mimic this behaviour. The fact that the relevant range of intensities is small lends support for our use of a linear approximation.

Assuming that an effective screen owing to abundant neutral hydrogen blocks photons in the Lyman-series lines from all sources at redshifts above $z_{\rm max}$ (Haiman et al. 1997), we can approximate $J_{\rm LW}$ at each redshift z_i by summing the emissivity in the LW band from all previously active sources up to $z_{\rm max}$. For our analysis, we set $z_{\rm max} = z_{i-1}$ and approximate $J_{\rm LW}(z_i)$ as arising from the unattenuated radiation field purely from the set of sources in the previous time-step. Our assumption should be reasonable given the large amount of neutral hydrogen present around the time when $J_{\rm LW}$ becomes appreciable and the fact that photons with $E = 13.6$ eV will be redshifted out of the relevant energy range (11.18–13.6eV) after $\sim$18 per cent change in redshift. Since the luminosity in the LW band per unit stellar mass for very massive stars is $L_{\rm LW} \simeq 3 \times 10^{21}$ erg s^{-1} Hz^{-1}M$^{-1}_{\odot}$, with only a weak dependence on the stellar mass, our expression for $J_{\rm LW}(z_i)$ becomes

$$J_{\rm LW}(z_i) = \frac{c}{4\pi} L_{\rm LW} \times M_{\star}^{\rm tot}(z_{i-1}) \times \Delta t_i \times V_{\rm box}^{-1}(z_i), \tag{5}$$

where c is the speed of light, $M_{\star}^{\rm tot}(z_{i-1})$ is the total star mass which was switched on at redshift step z_{i-1},Δt_i is our time-step of 3×10^6 yr and $V_{\rm box}^{-1}(z_i)$ is the proper volume of our simulation box at z_i.

Owing to the highly uncertain nature of shielding processes, we refrain from developing a complex parametrization of this effect (see, however, section 7.2 of Yoshida et al. 2003c). Rather, we adopt the conservative value of $K_{\rm shield} = 0.10$ as our maximum shielding effectiveness for haloes with $M_{\rm SF} > 10^5$ M$_{\odot}$ and linearly scale this value with mass such that $K_{\rm shield} = 1$ for $M_{\rm SF} \leqslant 10^3$ M$_{\odot}$ (corresponding to zero shielding). We apply this level of shielding in all our models.

Finally, we turn to the effect of metal pollution from the life-cycles of the first stars. Metals can cool gas inside haloes to temperatures lower than can be achieved by H_2 cooling, making possible the

formation of less massive *ordinary* population II stars. The critical transition between the two populations should occur after a certain level of metal enrichment has occurred. Assuming that the metallicity in the IGM is directly linked to the amount of gas that has been incorporated into population III stars, one can parametrize when this transition should occur in terms of the fraction of total gas that forms massive stars. Oh et al. (2001b) estimate that the critical transition should occur when a fraction of 3×10^{-5}–1.2×10^{-4} is formed into massive stars in the range 150–250 $M_\odot$, which are believed to be the main contributors of metals. It should be noted, however, that this estimate assumes that metals produced by massive stars are uniformly mixed throughout the IGM, which is unlikely. If this is not the case, and metals remain preferentially near sites of halo formation, then we would expect that the critical fraction is potentially much lower than the value reported by Oh et al. (2001b). In addition, stars with masses larger than 250 $M_\odot$ were excluded under the assumption that their contribution to metal enrichment should be small if they end their lives as black holes. However, the amount of mass these stars shed before they collapse into black holes is still relatively uncertain and may also reduce the fraction quoted above.

Given the large uncertainty associated with this fraction, we allow all our models to continually form population III stars all the way to $z = 16$ where we stop our simulations owing to the growing non-linearity of the fundamental fluctuation mode. For all the models which we consider, the fraction of total gas mass that is converted to stars $F_{\rm conv}$ by $z = 16$ falls short of the lower bound of the critical range quoted by Oh et al. (2001b). In an effort to study more protracted population III epochs, we will employ simple extrapolations of the model results to lower redshifts. This will allow us to assess the impact of population III stars for larger $F_{\rm conv}$ values more consistent with the critical range quoted in Oh et al. (2001b) (see Section 4.3).

3.3 Models

Our goal of identifying the important features which are associated with the ability of population III stars to reionize the Universe leaves us with a rather large parameter space to explore. Namely, even neglecting uncertainties associated with the LW background and metal enrichment, we are still left with four free parameters: $f_{\rm esc}$, $E_{\rm SF}$, $D_{\rm f}$, and $K_{\rm recup}$. Our approach of considering both a weak and strong case for each of these parameters thus leads to 16 separate models, which we list in Table 1.

In addition, we include a further model M9 which will represent our most restrictive case, where we allow only a single 200-$M_\odot$ star to form in each halo which has at least 4×10^4 $M_\odot$ of star-forming mass ($E_{\rm SF} = 0.005$). This model is meant to be more consistent with the picture described by Abel et al. (2002) who have used high-resolution hydrodynamical simulations to show that a pre-galactic halo tends to form only a single collapsing core in its centre without renewed fragmentation. In an effort to simulate the ultimate inhibition of subsequent star formation in these haloes, we further restrict the model to allow only one episode of population III star formation per halo without the possibility of forming new metal-free in the same halo or its descendants at a later time. In this case, once a single source turns on within the halo or its gas becomes ionized by a neighbouring source, we inhibit it from hosting any future metal-free stars ($D_{\rm f} = \infty$, $K_{\rm recup} = \infty$). It is important to point out that the total number of ionizing photons released by a single 200 $M_\odot$ star in the course of 3×10^6 yr easily exceeds the amount of baryons in even our most massive haloes and therefore justifies our use of relatively large escape fractions in single-star haloes (see Whalen et al. 2003).

Table 1. Models.

Model	$f_{\rm esc}$	$E_{\rm SF}$	$D_{\rm f}$	$K_{\rm recup}$
$M1_{(a,b)}$	$(0.3)_a$ $(1.0)_b$	0.02	40	1/3
$M2_{(a,b)}$	$(0.3)_a$ $(1.0)_b$	0.02	120	1/3
$M3_{(a,b)}$	$(0.3)_a$ $(1.0)_b$	0.005	40	1/3
$M4_{(a,b)}$	$(0.3)_a$ $(1.0)_b$	0.005	120	1/3
$M5_{(a,b)}$	$(0.3)_a$ $(1.0)_b$	0.02	40	2/3
$M6_{(a,b)}$	$(0.3)_a$ $(1.0)_b$	0.02	120	2/3
$M7_{(a,b)}$	$(0.3)_a$ $(1.0)_b$	0.005	40	2/3
$M8_{(a,b)}$	$(0.3)_a$ $(1.0)_b$	0.005	120	2/3
$M9_{(a,b)}$	$(0.3)_a$ $(1.0)_b$	0.005	∞	∞

The main goal of our analysis will be to explore the effectiveness of population III stars as ionizing sources in the early Universe. By considering a plausible set of models which incorporate feedback effects to varying degrees, we develop a better qualitative understanding of the complex interplay between these processes and reionization. Our inclusion of an *ultra-restrictive* model will allow us to constrain loosely the minimum effectiveness of population III reionization.

4 RESULTS AND DISCUSSION

The reionization history of H I and He II is followed in each of our models using the radiative transfer code described in Paper I. Briefly, radiative transfer is performed on a Cartesian grid with 200^3 cells using an adaptive ray-casting scheme (Abel & Wandelt 2002). Density fields, clumping factors, and source characteristics are taken from outputs of the hydrodynamic simulations; thus we neglect the dynamical feedback of the radiation on structure formation.[2] However, to account for the neglected photoheating of the IGM, we compute recombinations in our radiative transfer calculations according to an artificially raised temperature of $T = 1.5 \times 10^4$ K. This temperature corresponds to a reasonable estimate of the IGM temperature after reionization by sources with spectra typical of metal-free sources (Hui & Haiman 2003). If the photoionized gas has a higher temperature, recombinations occur at a slightly slower rate (the recombination time $t_{\rm rec} \propto T^{0.7}$) and ionization zones grow marginally faster. For lower temperatures, the opposite is true.

In the context of reionization studies, cosmic variance limits our ability to capture both a representative mass function for source haloes and also a reliable picture of the distribution of gas in the Universe. Since our simulation box has a comoving length of only 1 Mpc, we will not be able to make very strong statements regarding the precise moment of cosmic reionization. However, as stated earlier, our goal is only to assess the relative properties of a set of physically motivated models for the impact population III sources can have on reionization. Having stated this, we note that the same small box simulation was analysed in Yoshida et al. (2003a) and was found to contain halo abundances for $M > 7 \times 10^5$ $M_\odot$ that were in reasonable agreement with the Press–Schechter mass function between $17 < z < 25$ (see also Jang-Condell & Hernquist 2001). The incomplete sampling of the halo mass function owing to the finite box size is appreciable only at $z > 30$. However, as we shall show, star formation in our models is not dominated by rare massive

[2] See Sokasian, Abel & Hernquist, (2001) for a more detailed description of how we integrate radiative transfer calculations with existing outputs from cosmological simulations.

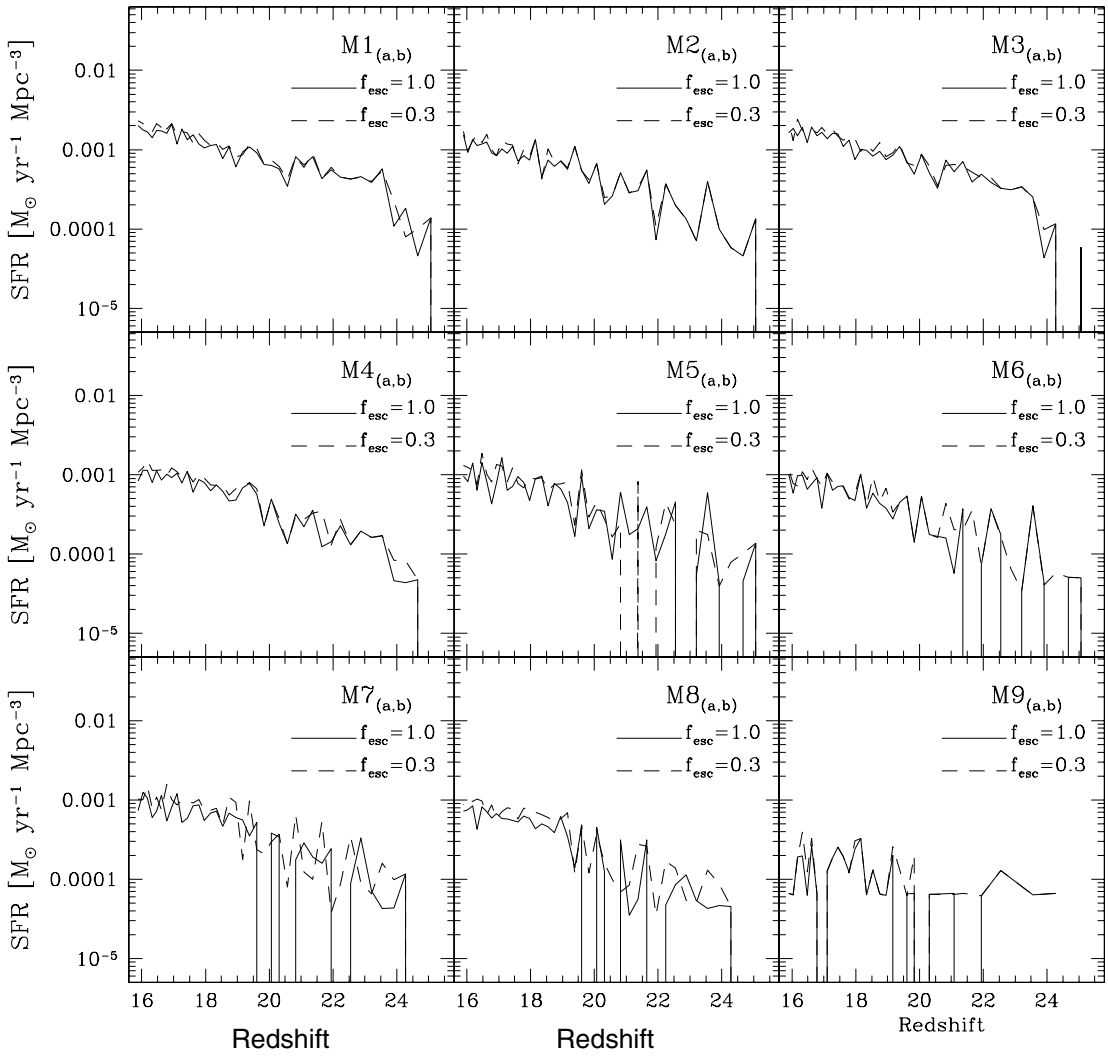

Figure 3. Evolution of the star formation rate density in each model down to $z = 16$.

haloes and therefore simulating larger volumes should not significantly alter our results.

4.1 Star formation history

In Fig. 3, we show the evolution of the star formation rate (SFR) density for population III stars for all our models. Here the SFR is computed on the fly as the simulation regulates the amount of star mass that actually turns on after incorporating the effects of feedback. By $z = 16$, all but our most restrictive model M9 appear to reach a SFR near 10^{-3} $M_\odot$ yr^{-1} Mpc^{-3}. The similarity in the SFRs between the different models brings attention to the self-regulating consequences of feedback. For example, when the disruption factor is large, less star formation takes place locally, which in turn minimizes negative feedback in the form of dissociating radiation and photo-evaporation. As a result, star formation is promoted externally and the global SFR is regulated. In a similar fashion, models with a low escape fraction limit the effect of photo-evaporation externally and therefore are able to have a similar level of star formation as models with a large escape fraction. In Section 4.3 we shall take a more detailed look at dynamic feedback and attempt to quantify the effect.

Nevertheless, it is important to point out that a SFR of 10^{-3} $M_\odot$yr^{-1} Mpc^{-3} is roughly an order of magnitude lower than the 'normal-mode' (population II) star formation predictions from Springel & Hernquist (2003) and Hernquist & Springel (2003) at the same redshift. Here, 'normal mode' refers to star formation occurring in larger mass systems where gas cooling takes place via atomic hydrogen and helium transitions and the only form of regulating feedback is supernovae. Besides the difference in amplitude, the SFR in our population III models appears to have relatively 'flatter' shapes in the range $16 < z < 20$ compared with the 'normal-mode' SFR of Hernquist & Springel (2003). This is not surprising given the stronger regulating processes associated with population III star formation. The overall shape and the amplitude of the SFR are in reasonable agreement with the semi-analytic prediction of Yoshida et al. (2003c, their fig. 18). It is important to note that population III star formation at $z \lesssim 20$ may have a significant impact on subsequent 'normal-mode' star formation occurring in small protogalaxies which are susceptible to the negative feedback effects of photoheating. Because these effects were not included, it is not surprising that the population III SFR presented here does not converge with the 'normal-mode' SFR of Hernquist & Springel (2003). Nevertheless, if the epoch of population III stars ends abruptly, as we have assumed here, then the transition itself should also be abrupt.

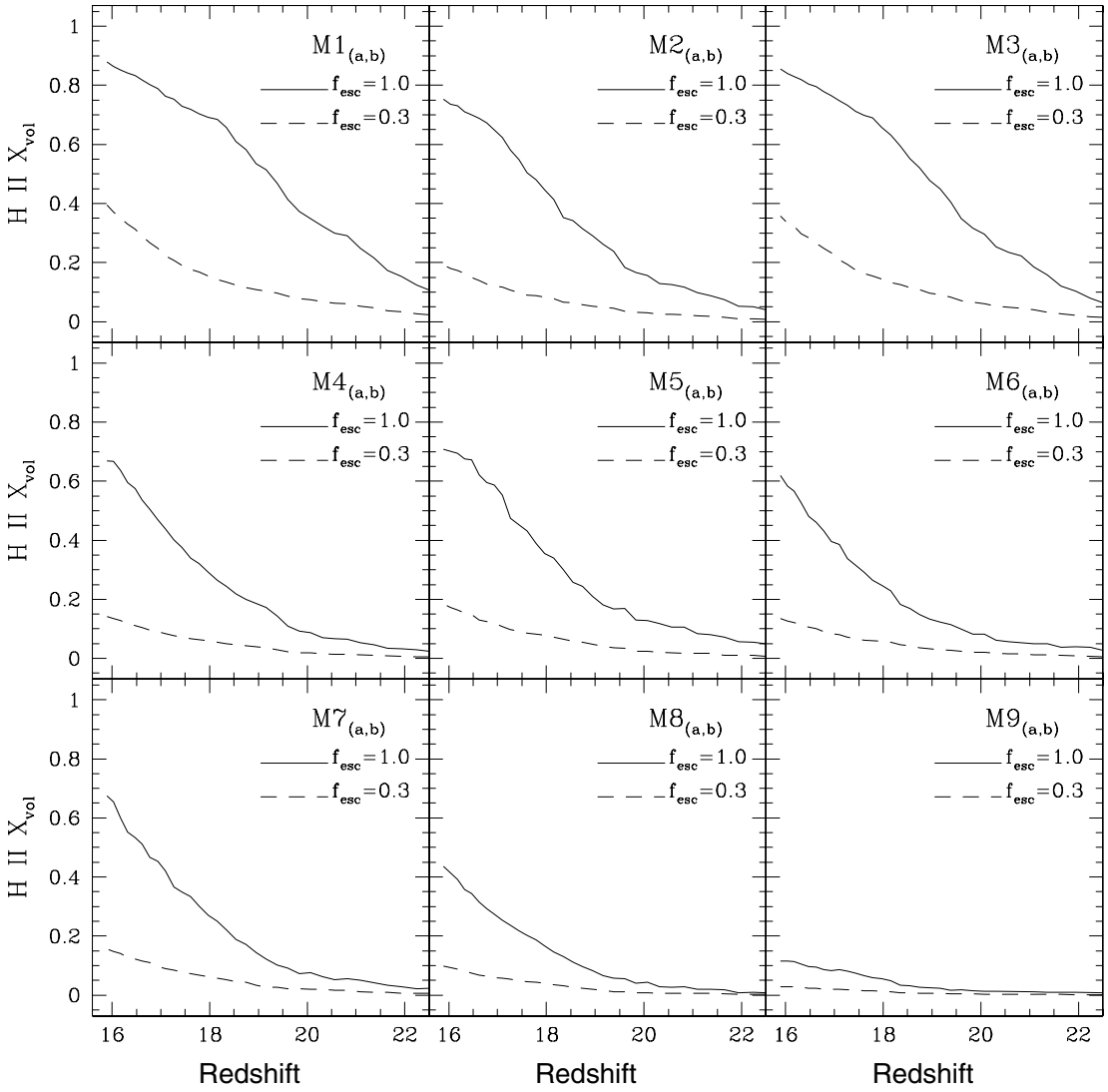

Figure 4. Evolution of the volume-weighted ionization fraction for H II in each model down to $z = 16$.

A very interesting issue for future work, therefore, would be to address how the transition from population III stars to ordinary star formation occurs. The discontinuity presented here represents an additional uncertainty of our analysis only when we attempt to compute a complete history of reionization which spans both population II and population III stars.

4.2 Global ionization fractions

The evolution of the global ionization fraction in the simulation volume is a useful tool for characterizing differences between the various models. In Figs 4 and 5, we show the evolution of the volume-weighted ionization fraction down to $z = 16$ for H II and He III, respectively. In each panel, we plot both the $f_{\rm esc} = 1.0$ (*solid-line*) and $f_{\rm esc} = 0.3$ (*dashed-line*) cases for the corresponding model. Here, we note that with the exception of our most restrictive model M9, all the $f_{\rm esc} = 1.0$ models are able to ionize their volumes significantly by $z = 16$. Interestingly, some of the models with higher emissivity are also able to doubly ionize helium substantially, although the corresponding fractions are much less than in H II. This is true despite the fact that the ionizing spectrum of a typical $300 - {\rm M}_{\odot}$ metal-free star produces roughly $\sim$3 times more ionizing photons per helium atom compared with hydrogen for cosmic abundances. The difference in the resultant ionization fractions owes to the fact that the recombination rate of He III is much larger relative to H II. This large recombination rate is also responsible for making He III ionization evolution relatively less smooth, because relic He III regions are much quicker to recombine.

In all our models, the initial rise of the ionization fraction appears to be closely correlated with the exponential growth of star-forming haloes in the volume. Interestingly, however, our highest emissivity models ($M1_b$, $M2_b$, $M3_b$) appear to show some degree of divergence from this rate at later times. In particular, the rise of the ionization fraction becomes shallower once the ionization fraction exceeds $\sim$60 per cent. The mostly likely explanation for this behaviour is that dynamic external feedback becomes particularly inhibitive once a substantial portion of the volume has become ionized and many sources become involved in the process. We will explore this effect in more detail in the next section where we try to assess the impact from this dynamic component of the feedback in terms of the amount of star mass that actually turns on at each time-step.

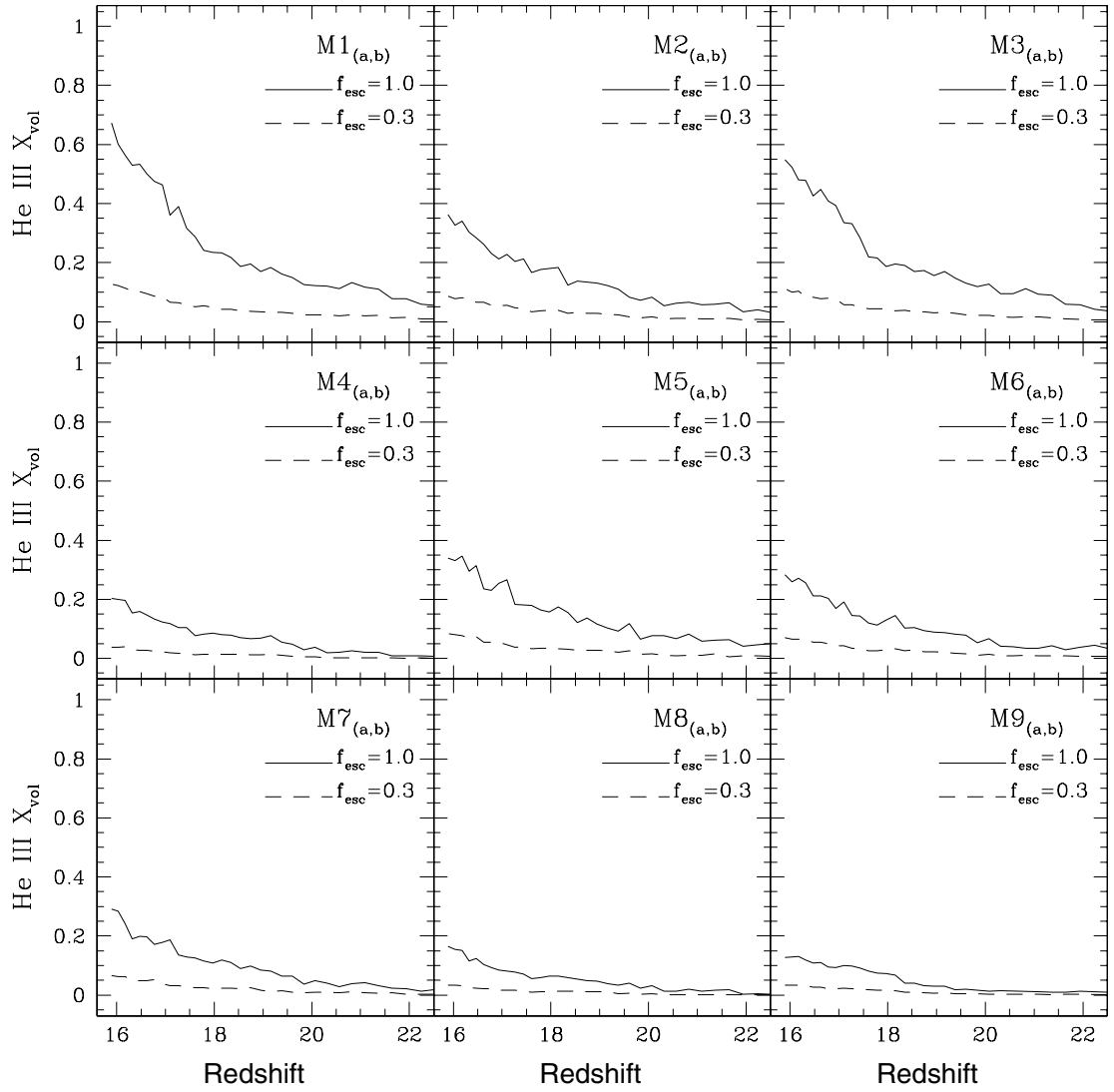

Figure 5. Same as Fig. 4, but for He III.

Table 2. Summary of model results at $z = 16$.

Model	$F_{\rm conv}$	$\sum$H II photons per H atom	$\sum$He III photons per He atom	H II $X_{\rm vol}$	He III $X_{\rm vol}$
$M1_{(a,b)}$	$(2.3e\text{-}05)_a$ $(2.1e\text{-}05)_b$	(0.87) (2.64)	(2.16) (6.59)	(0.39) (0.88)	(0.13) (0.67)
$M2_{(a,b)}$	$(1.5e\text{-}05)_a$ $(1.4e\text{-}05)_b$	(0.56) (1.71)	(1.36) (4.18)	(0.19) (0.75)	(0.09) (0.36)
$M3_{(a,b)}$	$(2.2e\text{-}05)_a$ $(1.9e\text{-}05)_b$	(0.79) (2.39)	(1.95) (5.93)	(0.36) (0.85)	(0.11) (0.55)
$M4_{(a,b)}$	$(1.4e\text{-}05)_a$ $(1.2e\text{-}05)_b$	(0.44) (1.28)	(0.94) (2.82)	(0.14) (0.67)	(0.04) (0.20)
$M5_{(a,b)}$	$(1.4e\text{-}05)_a$ $(1.2e\text{-}05)_b$	(0.51) (1.50)	(1.25) (3.71)	(0.18) (0.71)	(0.08) (0.34)
$M6_{(a,b)}$	$(1.1e\text{-}05)_a$ $(9.6e\text{-}06)_b$	(0.41) (1.16)	(0.99) (2.82)	(0.13) (0.62)	(0.07) (0.28)
$M7_{(a,b)}$	$(1.3e\text{-}05)_a$ $(1.0e\text{-}05)_b$	(0.45) (1.23)	(1.08) (2.98)	(0.16) (0.67)	(0.07) (0.29)
$M8_{(a,b)}$	$(9.9e\text{-}06)_a$ $(7.8e\text{-}06)_b$	(0.32) (0.86)	(0.70) (1.94)	(0.10) (0.44)	(0.03) (0.16)
$M9_{(a,b)}$	$(2.4e\text{-}06)_a$ $(1.9e\text{-}06)_b$	(0.09) (0.24)	(0.22) (0.59)	(0.03) (0.12)	(0.03) (0.13)

A summary of the ionization results at $z = 16$ is given in Table 2, which lists for each model the fraction of total gas mass converted to stars $F_{\rm conv}$, the cumulative number of ionizing photons released per atom and the volume ionization fraction for H II and He III, respectively. Here we point out that while our more restrictive models do not achieve as high an ionization fraction as the models with larger emissivities by $z = 16$, they convert less gas mass into stars and therefore should have polluted their environment relatively less with metals. As a result, we would expect that metal-free star formation should persist longer in these models. It is particularly interesting to compare the results for our most restrictive model M9 to our most liberal model M1. We note in particular that the

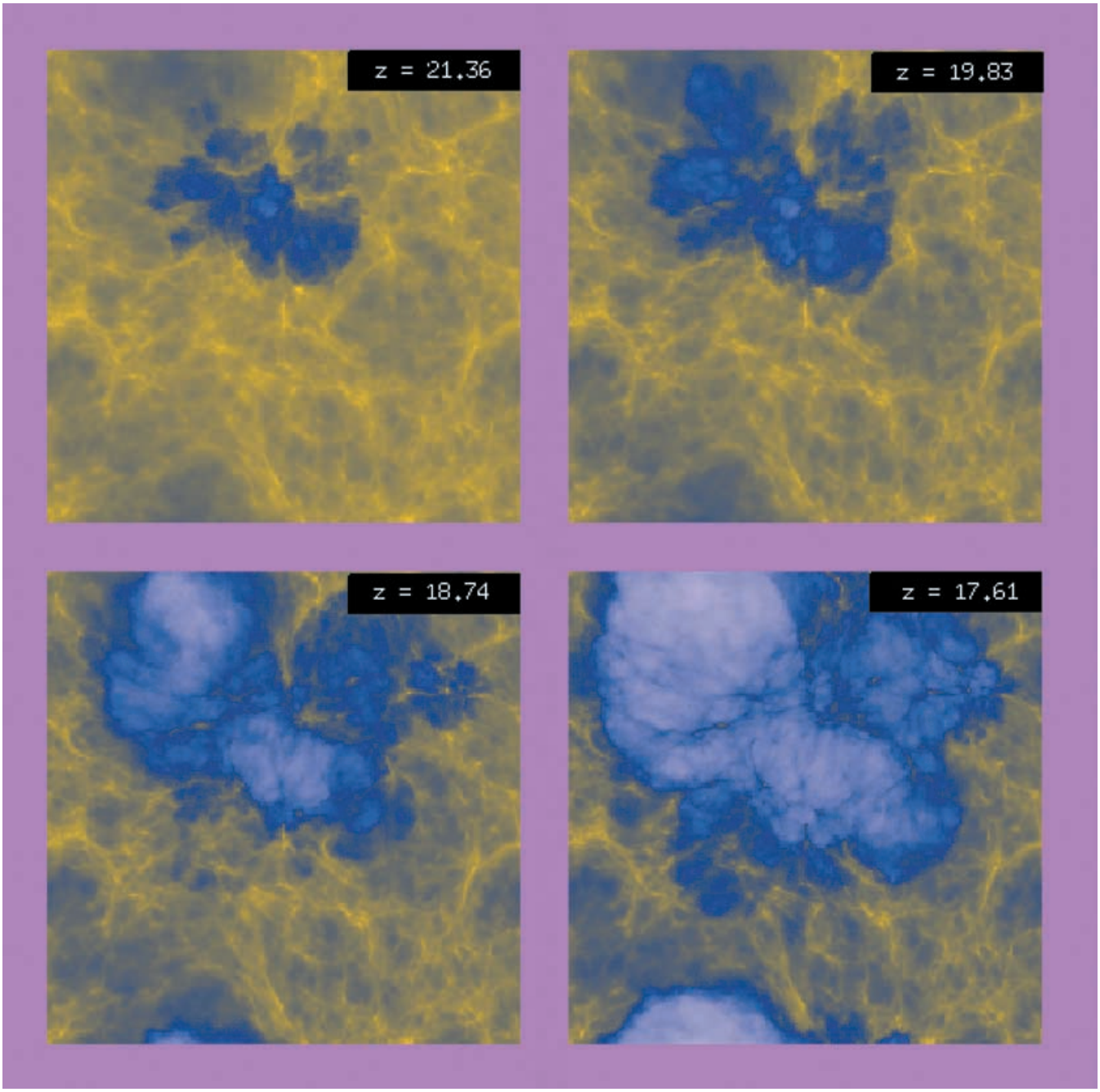

Figure 6. A series of projected slices through the simulation volume at (*top left* to *bottom right*) $z = 21.4$, 19.8, 18.7, and 17.6. In each panel, a 0.25-Mpc slice (1/4 of the box length) from the outputs of the $M1_a$ ($f_{esc} = 1.0$) model is projected in both density and ionization fraction. From the plots one can follow the growth of the ionization zones (*blue*) around the first stars as they turn neutral gas (*yellow*) into highly ionized regions (*light blue*).

realization of a 'one-star-per-halo' for metal-free stars as defined in our M9 model has such a slow rate of growth for its ionizing emissivity that recombinations will likely prevent the ionization fraction from increasing significantly even if we had extended this model down to lower redshifts. However, we point out that this model is relatively more efficient in terms of the resultant ionization fraction per ionizing photon than the M1 model with larger emissivity. This feature can be attributed to the fact that models with higher emissivity suffer cumulatively more recombinations as a result of ionizing substantial portions of their volumes at very early redshifts and keeping them ionized down to lower redshifts. It should be noted, however, that this difference will be slightly diminished by the fact that ionization fronts in the more restrictive M9 model have difficulty breaking through the dense environments surrounding the sources. This causes the M9 model to suffer relatively more recombinations *per unit volume* than models with higher emissivity, the ionization zones of which expand into the less dense and more voluminous portions of the IGM. This morphological effect also helps to explain why models M4–M9, which have not yet experienced a slow-down in the rate of ionizing photon production (owing to external feedback factors), exhibit ionization fractions for their $f_{esc} = 0.3$ case that are systematically lower than 0.3 times the

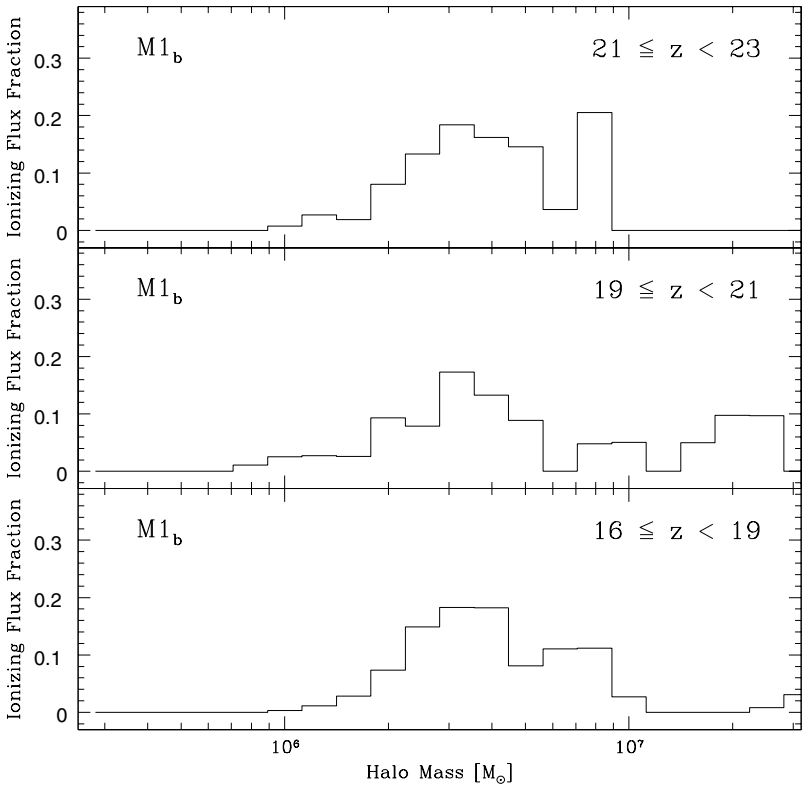

Figure 7. The fraction of total ionizing flux released by population III stars in model $M1_b$ as a function of halo mass for redshift ranges $21 \leqslant z < 23$, $19 \leqslant z < 21$, and $16 \leqslant z < 19$. Similar results were obtained for models M2–M9.

ionization fractions predicted in the corresponding $f_{\rm esc} = 1.0$ case (see Table 2).

A visual illustration of the reionization process is shown in Fig. 6 where we plot a series of projected slices through the simulation volume from the $M1_a$ model (other models exhibit a similar topological evolution in their ionization structures). In each panel, a 0.25-Mpc slice is projected in both density and ionization fraction. From the plots one can follow the growth of the ionization zones (*blue*) around the first stars as they turn neutral gas (*yellow*) into highly ionized regions (*light blue*). The plots clearly show the preferential advance of ionization fronts into the underdense regions, responsible for the steep rise seen in the corresponding volume-weighted ionization fractions.

To understand which haloes are contributing the bulk of the ionizing radiation, we plot in Fig. 7 the fraction of ionizing flux released as function of halo mass for three redshift ranges associated with the $M1_b$ run (other models had similar results). Here we see that through the redshift ranges $21 \leqslant z < 23$, $19 \leqslant z < 21$, and $16 \leqslant z < 19$, the bulk of ionizing radiation is consistently released from haloes with masses between $\sim 2 \times 10^6$ $M_\odot$ and $\sim 6 \times 10^6$ $M_\odot$. The fact that these 'mini-haloes' are capable of substantially ionizing the IGM appears to contrast with the findings of Ricotti et al. (2002a), who conducted similar 3D cosmological simulations which included dynamically linked radiative transfer calculations (see Ricotti et al. (2002b) for simulation details). They showed that negative feedback prevents the size of H II regions from exceeding the size of the dense filaments; hence, 'mini-haloes' are not able to reionize the voids. More specifically, the Ricotti et al. (2002a) simulations showed that positive feedback from the accelerated formation rate of molecular hydrogen in front of ionization fronts within these filaments provided an effective shield preventing the destruction of molecular hydrogen in other star-forming regions. On the contrary, when the ionization fronts expand beyond the filaments, densities drop and the shield disappears allowing negative feedback from LW radiation and photoevaporation to dominate. Ricotti et al. (2002a) thus concluded that the volume filling factor of the H II regions associated with these 'mini-haloes' remains small and cannot reionize the Universe.

Although none of the models considered in our analysis is able to reionize the Universe fully before the onset of population II stars, they do ionize a substantial portion of the IGM. This discrepancy most likely results from the way in which negative feedback is treated in the simulations. More specifically, by dynamically linking approximate radiative transfer calculations directly with cosmological simulations, Ricotti et al. (2002a) are able to simulate positive feedback processes preceding H II regions, which effectively reduces negative feedback from the dissociation of molecular hydrogen. However, when the ionizing emissivity of 'mini-haloes' is large, ionization fronts expand outside of the filaments and negative feedback from dissociation and photo-heating begins to dominate. Since our analysis does not allow us to couple radiative transfer effects directly into the cosmological simulations, we are unable to include positive feedback effects such as the one mentioned above. Nevertheless, the models we consider are able to easily force ionization fronts beyond the dense filaments and therefore we do not expect positive feedback to be important in these cases. Once ionization fronts expand into the IGM, negative feedback effects kick in through our ad hoc implementation of the photo-evaporation effect and the LW dissociating background. As we shall show in the following section, such feedback works to regulate further star formation, however, unlike Ricotti et al. (2002a) we do not find that it suppresses star formation fully. It is important to note that our

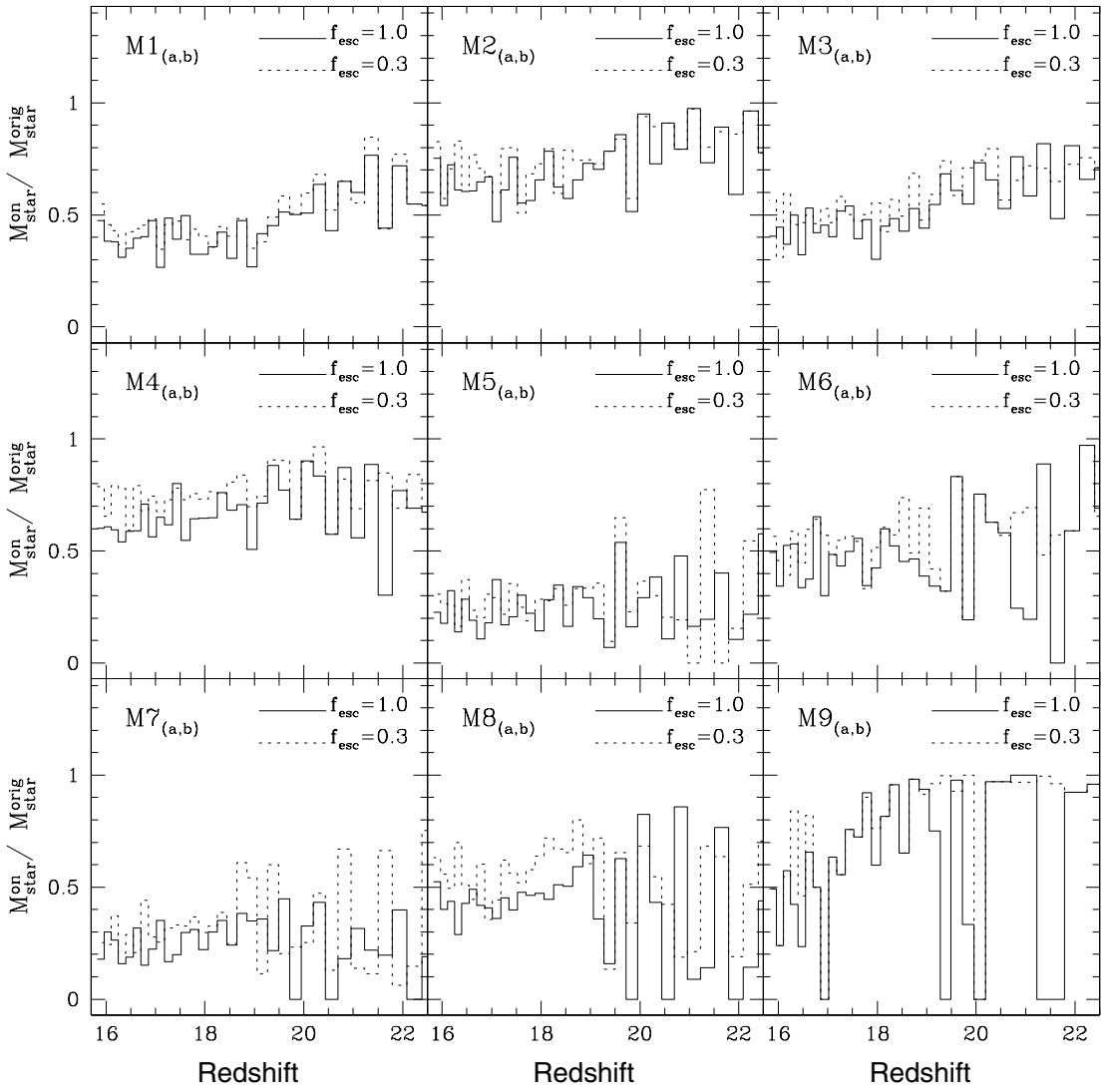

Figure 8. The evolution of the ratio of the star mass that actually turns on at each time-step $M_{\rm star}^{\rm on}$ to the star mass originally available $M_{\rm star}^{\rm orig}$ before the effects of the LW background and the 'ionization exclusion effect' were taken into account (see Table 3 for related statistics).

simulations included an approximate treatment that allowed haloes to shield themselves against dissociating radiation in proportion to their masses. In contrast, self-shielding was excluded in the simulations of Ricotti et al. (2002a) and may have resulted in an overestimation of negative feedback, plausibly causing much of our discrepancy with the results of Ricotti et al. (2002a). Furthermore, it should be pointed out that the discrepancy may also be related to a number of other differences between the two simulations such as the differing methodologies used in the calculation of the star-forming mass in the haloes as well as differences in the choice of the IMF.

4.3 Dynamical feedback from the LW background and photo-evaporation

In Figs 4 and 5 we showed the evolution of the global volume-weighted ionization fraction for each model. While useful for making comparisons between the net ionizing ability of the models, the figures do not reveal the complex role dynamical feedback may have played in the evolution. In this section we attempt to study the effectiveness and subsequent evolution of this feedback more directly. In particular, we focus on tracking the modulating behaviour of our implementation of the LW background and the photo-evaporation effect (or in terms of our parametrization, the 'ionization exclusion effect'). More specifically, by tracking the ratio of the star mass that actually turns on at each time-step $M_{\rm star}^{\rm on}$ to the star mass originally available $M_{\rm star}^{\rm orig}$ (computed in the absence on any external feedback), we can directly study the net impact from both these effects. In Fig. 8 we show the ratio $M_{\rm star}^{\rm on}/M_{\rm star}^{\rm orig}$ at each redshift step as a histogram for all our models. The plots reveal sharp swings, mainly owing to the discrete time-steps used. However, these swings are enhanced at early times, reflecting the strong nature of our 'ionization exclusion effect' when localized to a small region with only a few sources, which is the case when the first cluster of sources turns on. As more sources are invoked at lower redshifts, this ratio begins to behave more smoothly.

In Table 3 we list for all the models the mean value of $M_{\rm star}^{\rm on}/M_{\rm star}^{\rm orig}$ weighted by the original star mass between the time the first source turns on and $z = 16$. This mass-weighted mean quantifies the relative effectiveness of external dynamical feedback. Note, in particular, how models in which we have incorporated strong local feedback

Table 3. Mean fraction for dynamic modulation of star mass.

Model	mean$[\frac{M_{\rm star}^{\rm on}}{M_{\rm star}^{\rm orig}}]_{\rm mass-weighted}$
$M1_{(a,b)}$	$(0.46)_a$ $(0.44)_b$
$M2_{(a,b)}$	$(0.67)_a$ $(0.62)_b$
$M3_{(a,b)}$	$(0.54)_a$ $(0.48)_b$
$M4_{(a,b)}$	$(0.68)_a$ $(0.56)_b$
$M5_{(a,b)}$	$(0.28)_a$ $(0.24)_b$
$M6_{(a,b)}$	$(0.48)_a$ $(0.41)_b$
$M7_{(a,b)}$	$(0.33)_a$ $(0.28)_b$
$M8_{(a,b)}$	$(0.50)_a$ $(0.39)_b$
$M9_{(a,b)}$	$(0.59)_a$ $(0.41)_b$

effects have correspondingly low values for this mean ratio (compare, for example, models M1↔M2 and M3↔M4). This is a clear indication of the self-regulating feature of the population III era: when local negative feedback is strong, the global component of negative feedback is reduced, allowing for more sources to turn on in distant regions. This feature helps to explain how such a large set of model realizations leads to the relatively similar ionization histories seen in Figs 4 and 5.

Bearing in mind that the net effect of the LW background is to systematically reduce $M_{\rm star}^{\rm on}/M_{\rm star}^{\rm orig}$ in proportion to the star mass that forms, one can use the mean of this ratio to isolate and assess the relative impact of the photo-evaporation effect between the models M1↔M5, M2↔M6, M3↔M7, and M4↔M8. Note in particular, the significant drop in this ratio from M1→M5, which gives an indication that external feedback may play an important role in scenarios where star formation is efficient and internal feedback is low.

Interestingly, the effectiveness of external feedback is strong by $z \sim 16$ even in model M9 which turns on very few sources. This is most likely owing to the fact that these sources reside in only the most clustered regions containing massive enough haloes capable of hosting sources in this *ultra-restrictive* model. The close proximity of the sources to one another in these regions therefore keeps external feedback in the form of photo-evaporation particularly effective in inhibiting a fair portion of the sources from turning on. We mention that, under certain conditions, weak ionizing radiation can promote molecular hydrogen formation and enhance primordial gas cooling, hence causing possibly *positive* feedback effects (Haiman et al. 1996; Kitayama et al. 2001). We do not consider the effects in our models and thus all the models may be restrictive in this sense.

4.4 Electron optical depth: population II and III sources

The recent tentative measurement of polarization in the CMB by the *WMAP* satellite (Kogut et al. 2003) indicates that reionization occurred earlier than implied by the SDSS quasars alone (e.g. Spergel et al. 2003). The optical depth to Thomson scattering is $0.13 < \tau_e < 0.21$, corresponding to an instantaneous reionization epoch between $14 < z < 20$. In Paper I, we showed that stellar sources similar to those seen in local galaxies, i.e. population II type stars, are unable to reionize the Universe by such high redshifts. Meanwhile, the analysis in this paper indicates that metal-free (population III) stars could have significantly reionized the Universe at $z > 16$. Cen (2003a,b); and Wyithe & Loeb (2003a,b) explored a large number of models of reionization history using semi-analytic methods and argue that, in some specific cases, the Universe could be reionized twice.

In an effort to study this scenario more quantitatively, we would like to couple the ionization histories from both types of sources and compute the resulting integrated electron optical depth. Unfortunately, owing to the high resolution necessary for carrying out simulations involving population III stars, we are unable to include these sources directly in the larger simulation volumes necessary for studying cosmic reionization by population II sources (galaxies). We are therefore forced to adopt the more approximate approach of linking together the ionization histories from the two sets of simulation volumes. More specifically, our approach relies on using the results of our population III simulations to estimate the volume-weighted ionization fraction at redshifts around which it is reasonable to assume that star-forming haloes have exhausted their ability to form additional metal-free stars. At this point in time, we then rerun the $f_{\rm esc} = 0.20$ population II simulation from Paper I (conducted in a 14.3 Mpc comoving box) with the initial conditions that the IGM was *uniformly* ionized to the same ionization fraction (both in hydrogen and helium) as estimated by our population III simulations and also *uniformly* heated to $T = 1.5 \times 10^4$ K. Our use of this particular model for population II sources is motivated by our analysis in Paper I where we found that given the amplitude and form of the underlying star formation predictions, an escape fraction near 20 per cent is most successful in terms of statistically matching observational results from the $z = 6.28$ SDSS quasar of Becker et al. (2001) (see Paper I for further details). By linking together the two simulations in this fashion, we are assuming that the onset of population II begins exclusively at redshifts below the transition redshift and that there are no population III stars thereafter. Since the relative contribution predicted for population II sources in the simulations is small above the transition redshifts which we will consider, we can reliably separate the two contributions in this manner.

Given the fact that most of our population III models ionize the volume to a similar extent by $z = 16$, we are motivated to simplify our analysis by grouping together these models into a single model by averaging all the results at each redshift. We perform this averaging for models M1–M8, but continue to keep model M9 distinct as it represents our *ultrarestrictive* case which predicts significantly lower ionization fractions as a result of invoking only a single 200 $M_\odot$ star once per star-forming halo. By $z = 16$, at which point we stop our population III simulations, our combined model M1–M8 with $f_{\rm esc} = 0.30$ ($f_{\rm esc} = 1$) has converted a fraction $F_{\rm conv} = 1.53 \times 10^{-5}$ ($F_{\rm conv} = 1.26 \times 10^{-5}$) of its total gas into stars. This fraction falls short of the lower limit estimated by Oh et al. (2001b) for the transition to the population II epoch ($\sim 3 \times 10^{-5}$). In an effort to examine a more prolonged population III epoch culminating with gas-to-star conversion fractions more in line with the estimates from Oh et al. (2001b), we apply a simple extrapolation of all the simulation results to redshifts below $z = 16$. More specifically, we extrapolate the simulations using the associated rate of change in the models between $z = 18$ and $z = 16$. For the combined M1-M8 model with $f_{\rm esc} = 0.30$ ($f_{\rm esc} = 1$), we extrapolate the population III epoch down to $z = 14.5$ and $z = 12.0$ resulting in gas conversion fractions: $F_{\rm conv} = 2.20 \times 10^{-5}$ ($F_{\rm conv} = 1.90 \times 10^{-5}$) and $F_{\rm conv} = 3.32 \times 10^{-5}$ ($F_{\rm conv} = 2.86 \times 10^{-5}$), respectively. In the case of model M9 with $f_{\rm esc} = 0.30$ ($f_{\rm esc} = 1$), even an extrapolation down to $z = 12$ only yields a conversion fraction of $F_{\rm conv} = 5.10 \times 10^{-6}$ ($F_{\rm conv} = 3.94 \times 10^{-6}$), well below the estimate from Oh et al. (2001b). However at $z \lesssim 12$, population II stars that form via atomic line cooling in massive haloes begin to dominate the ionizing emissivity relative to the population III stars incorporated in M9. We therefore adopt $z =$

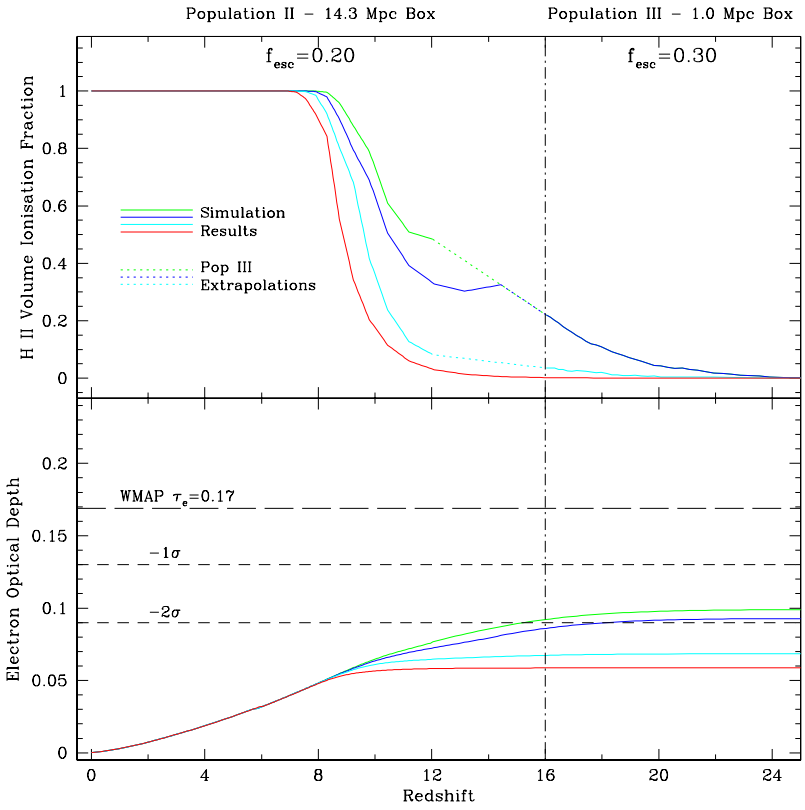

Figure 9. Top panel: the evolution of the H II volume-weighted ionization fraction obtained by linking together the ionization histories of $f_{\rm esc} = 0.30$ population III simulations with $f_{\rm esc} = 0.20$ population II simulations described in Paper I. Here the vertical dashed-dotted line represents the redshift ($z = 16$) where we were forced to stop our population III simulations owing to the small box size. The dotted lines extending below this redshift represent extrapolations of the ionization fraction if the population III epoch had continued to lower redshifts (see text for discussion). The models shown are (from top to bottom): (1) *blue line*: the combined (mean) population III simulation results from models M1a-M8a ($f_{\rm esc} = 0.30$) extrapolated down to $z = 14.5$ before switching to the ($f_{\rm esc} = 0.20$) population II simulation, (2) *green line*: same as (1) but with the population III epoch extrapolated down to $z = 12$. (3) *cyan line*: model M9a (*ultrarestrictive* 'one-star-per-halo' model) with a population III epoch extrapolated to $z = 12$ before switching to the population II simulation, and (4) (*red line*): the case where *only* population II sources are present (representing the $f_{\rm esc} = 0.20$ model from Paper I). Bottom-panel: corresponding optical depths to Thomson scattering $\tau_{\rm e}$ between the present and redshift z. The inferred value for $\tau_{\rm e}$ from the *WMAP* measurement is shown (*long-dashed line*) as is the corresponding 1σ and 2σ lower bounds (*short-dashed lines*).

12 as our epoch transition redshift for this model, keeping in mind that the exclusion of population III sources below $z = 12$ slightly underestimates the resultant rise in the global ionization fraction.

In Figs 9 and 10, we plot the evolution of the H II volume-weighted ionization fraction (*top-panel*) and the corresponding optical depth to Thomson scattering $\tau_{\rm e}$ between the present and redshift z (*bottom-panel*) for the models discussed above with $f_{\rm esc} = 0.3$ and $f_{\rm esc} = 1.0$, respectively. Here the vertical dashed-dotted line represents the redshift ($z = 16$) where we stop our population III simulations. The meaning of the various curves is summarized in the caption to Fig. 9. The electron optical depth was calculated from

$$\tau_{\rm e}(z) = \int_0^z \sigma_{\rm T} n_{\rm e}(z') c \left| \frac{{\rm d}t}{{\rm d}z'} \right| {\rm d}z', \qquad (6)$$

where $\sigma_{\rm T} = 6.65 \times 10^{-25}$ cm^2 is the Thomson cross-section and $n_{\rm e}(z')$ is the mean electron number density at z'. In the calculation of $\tau_{\rm e}$ we use mass-weighted ionization fractions and assume that helium is singly ionized to the same degree as the hydrogen component for $z > 3$ and doubly ionized everywhere at $z < 3$. The figure clearly demonstrates how population III sources may have significantly contributed to the electron optical depth, especially in the case where the escape fraction from the mini-haloes hosting metal-free stars is close to unity. Interestingly, the relatively late onset of population III stars does not cause a dramatic recombination era before population II stars begin to continue the reionization process.

Comparisons with the *WMAP* results show that only the combined model with $f_{\rm esc} = 1.0$ comes close to the inferred mean value of $\tau_{\rm e} = 0.17$ (*dashed line*) with optical depths 0.141 and 0.152 for population III extrapolations to $z = 14.5$ and $z = 12$, respectively. In the case of our *ultraconservative* M9 model with $f_{\rm esc} = 1.0$, the resultant optical depth is ∼40 per cent larger than in the case with only population II stars only, but is slightly shy of the lower 2σ limit of the *WMAP* measurement. In all cases, however, it appears that a large escape fraction is required during the population III epoch in order to contribute significantly to the integrated optical depth.

5 SUMMARY AND CONCLUSIONS

In this paper we have applied approximate radiative transfer calculations to the results of cosmological simulations capable of following early structure formation in an effort to study the potential impact that the first generation of metal-free stars may have had on the reionization history of the Universe. By incorporating a series of approximate feedback effects, we are able to simulate the complex interrelated processes which may have self-regulated subsequent population III star formation. We have examined a set of models

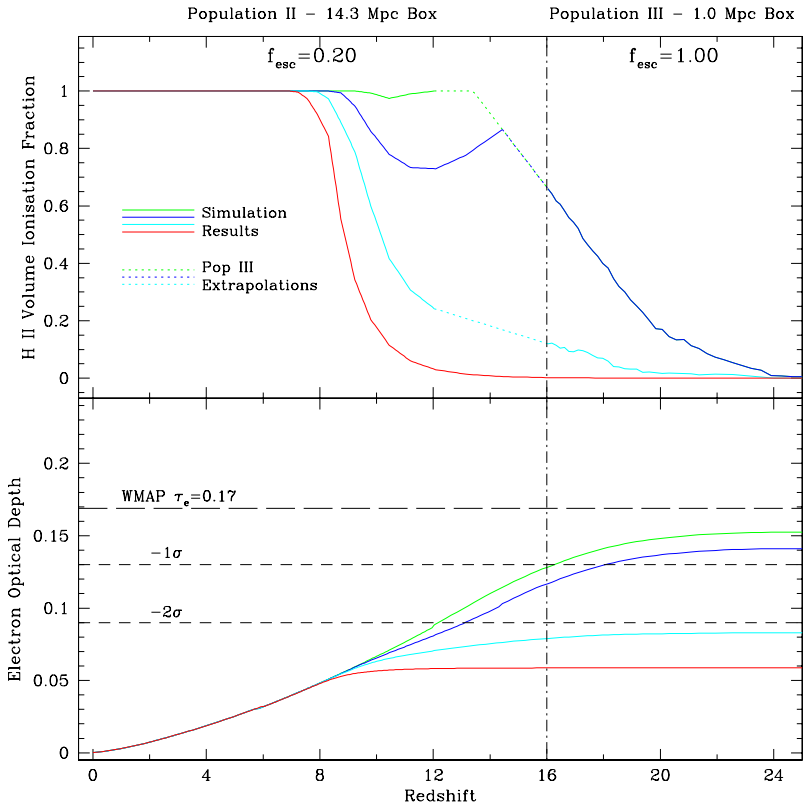

Figure 10. Same as Fig. 9 but for population III sources with $f_{\rm esc} = 1.0$.

in which the severity of the effects was varied in order to capture qualitatively how the feedback can affect star-formation at early epochs.

Overall, we find that for a plausible range of values related to our parametrizations, population III star formation proceeds in a self-regulated manner. As a result, the net impact of these sources in terms of reionization is fairly insensitive to the relative degree of severity of one form of feedback over another. This is true as long internal feedback within a halo is not exceedingly large and haloes can host multiple generations of population III stars. In particular, we find that if we restrict haloes of sufficient mass to host only a single 200-$M_\odot$ star *once* in their existence, then the impact of population III sources on reionization is significantly reduced.

In the models where there is no restriction on the number of stars a halo can host and the escape fraction is unity, the mean level of ionization reached by $z = 16$ is 66 per cent and 29*percent* for H II and He III, respectively. One would therefore expect that, at least within the context of this description, population III stars should have had a significant impact on the ionization history of the Universe. Interestingly, the fact that the helium component may also have been ionized to a significant fraction has consequences for the thermal history of the IGM (e.g. Hui & Haiman 2003) and could possibly be observable with future observations of He II recombination lines in the host haloes using the *Next Generation Space Telescope* (Oh, Haiman & Rees 2001a; Tumlinson, Giroux & Shull 2001).

By linking together the simulation results of the population II study from Paper I with the results of the population III analysis presented here, we are able to synthesize a full history of how the Universe may have been reionized. We find that even with fairly conservative estimates for negative feedback, population III sources with large escape fractions are able to significantly raise the total electron optical depth so that it becomes statistically consistent (within the 1σ lower bound) with the *WMAP* measurement. We note that the Thomson optical depths predicted in our analysis appear to be lower than those obtained in the semi-analytic treatment conducted by Cen (2003a). Correspondingly, population III sources in our analysis appear to significantly affect the reionization history of the Universe only at relatively later times ($z \lesssim 19$) than the models considered by Cen (2003a). Nevertheless, both studies appear to suggest that achieving $\tau_{\rm e} > 0.17$ seems quite difficult with reasonable assumptions for the properties of population III stars. It is impractical to make more direct comparisons between the two works given the very different approaches employed and the large number of parameters. It should also be noted that semi-analytic treatments do no allow for the direct incorporation of negative feedback effects and instead absorb these uncertainties directly into star formation efficiency factors. As a result, they may oversimplify the true impact of these effects if the amount of star mass that turns on in each halo is a sensitive function of halo properties such as proximity to other haloes, merger history, and total mass (Yoshida et al. 2003c).

In carrying out our analysis, we were forced to extrapolate a small portion of the population III ionization history to lower redshifts owing to box-size limitations. In doing so, we were able to produce gas-to-star conversion fractions which approached the critical range described in Oh et al. (2001b), estimated to mark the transition to the population II epoch. It is important to point out that the simple recipe of Oh et al. (2001b) may not accurately reflect the transitional stage if metal pollution is not efficient. In particular, in the case of an inefficient mixing mechanism, the metallicity in overdense regions

can almost reach solar levels even at $z > 16$ for a top heavy IMF, preemptively ending the population III epoch (e.g. Yoshida et al. 2003e). Nevertheless, in all of our models we switched over to a population II epoch at aggressively conservative values below or slightly above the lower bound of the estimated range in Oh et al. (2001b). Therefore, it is plausible that population III star formation continues beyond the transitional redshifts considered here. If that is the case, population III stars would continue to significantly ionize the IGM, potentially leading to a single reionization epoch in which population II sources turn on at relatively late times and are intense enough to keep the IGM in a highly ionized state. In fact, our combined $f_{\rm esc} = 1$ population III model, when extrapolated down to $z = 12$, exhibits such a single reionization epoch. Interestingly, the results from this model appear very similar to the prediction from our model in Paper I which incorporated an evolving ionizing boosting factor as an additional multiplicative factor to the intrinsic ionization rates in population II sources. Such an evolution would be indicative of an evolving IMF which became more and more top-heavy with increasing redshift. We note however, that such a 'vanilla' model of reionization may be inconsistent with the observational constraints from the thermal history of the IGM as noted earlier. Future observations of CMB polarization by the *Planck* surveyor, potentially tractable observations of the 21-cm emission signal from neutral hydrogen at high redshifts (see Furlanetto,Sokasian & Hernquist 2003; Ciardi & Madau 2003; Zaldarriaga, Furlanetto & Hernquist 2003), and searches for Lyα emission from galaxies at the reionization epoch (e.g. Barton et al. 2004) may help resolve these degeneracies.

Through our analysis, we have attempted to assess the potential role feedback effects may have had on the ability of population III sources to reionize the Universe. While our radiative transfer simulations capture nearly all the important physical mechanisms operating during reionization, the precise effects of some processes that are modelled in an ad hoc manner remain still uncertain. More accurate studies may soon be forthcoming with the incorporation of radiative transfer calculations directly into cosmological simulations similar to the one used here.

Finally, we emphasize that the results here were obtained for a conventional ΛCDM cosmology. If the true power spectrum is actually similar to the running spectral index (RSI) model advocated by Spergel et al. (2003), 'first star formation' in mini-haloes will be greatly suppressed (Yoshida et al. 2003a). It is an open question whether the first luminous sources at redshifts below $z \lesssim 18$ in a RSI cosmology can produce a Thomson optical depth consistent with the *WMAP* measurement.

ACKNOWLEDGMENTS

We thank Volker Bromm and Marie Machacek for insightful discussions related to this study. This work was supported in part by NSF grants ACI 96-19019, AST 98-02568, AST 99-00877, and AST 00-71019 and NASA ATP grants NAG5-12140 and NAG5-13292. NY acknowledges support from the Japan Society of Promotion of Science Special Research Fellowship. The simulations were performed at the Centre for Parallel Astrophysical Computing at the Harvard-Smithsonian Centre for Astrophysics.

REFERENCES

Abel T., Wandelt B. D., 2002, MNRAS, 330, L53
Abel T., Anninos P., Norman M. L., Zhang Y., 1997, New Astron., 2, 181
Abel T., Anninos P., Norman M. L., Zhang Y., 1998, ApJ, 508, 518
Abel T., Bryan G. L., Norman M. L., 2000, ApJ, 540, 39
Abel T., Bryan G. L., Norman M. L., 2002, Sci, 295, 93
Barkana R., Loeb A., 2001, Phys. Rep., 349, 125
Barton E. J., Davé R., Smith J. D. T., Papovich C., Hernquist L., 2004, ApJL, submitted (astro-ph/0310514)
Becker R. H. et al., 2001, AJ, 122, 2850
Bromm V., Coppi P. S., Larson R. B., 1999, ApJ, 527, L5
Bromm V., Coppi P. S., Larson R. B., 2002, ApJ, 280, 825
Bromm V., Ferrara A., Coppi P. S., Larson R. B., 2001a, MNRAS, 328, 969
Bromm V., Kudritzki R. P., Loeb A., 2001b, ApJ, 552, 464
Bromm V., Yoshida N., Hernquist L., 2003, ApJ, 596, L135
Cen R., 2003a, ApJ, 591, 5
Cen R., 2003b, ApJ, 591, 12
Ciardi B., Ferrara A., Abel T., 2000a, ApJ, 533, 594
Ciardi B., Ferrara A., Governato F., Jenkins A., 2000b, MNRAS, 314, 611
Ciardi B., Madau P., 2003, ApJ, 596, 1
Ciardi B., Stoehr F., White S. D. M., 2003, MNRAS, 343, 1101
Couchman H. M. P., Rees M. J., 1986, MNRAS, 221, 53
Dekel A., Rees M. J., 1987, Nat, 326, 455
Djorgovski S. G., Castro S. M., Stern D., Mahaba A., 2001, ApJ, 560, 5
Fan X. et al., 2000, AJ, 120, 1167
Fan X. et al., 2003, AJ, 125, 1649
Furlanetto S. R., Sokasian A., Hernquist L., 2003, MNRAS, 347, 187
Galli D., Palla F., 1998, A&A, 335, 403
Gnedin N. Y., 2000, ApJ, 535, 530
Haiman Z., Abel T., Rees M. J., 2000, ApJ, 534, 11
Haiman Z., Rees M. J., Loeb A., 1997, ApJ, 476, 458
Haiman Z., Rees M. J., Loeb A., 1996, ApJ, 467, 522
Heckman T. M., Sembach K. R., Meurer G. R., Leitherer C., Calzetti D., Martin C. L., 2001, ApJ, 558, 56
Heger A., Woosley S. E., 2002, ApJ, 567, 532
Hernquist L., Springel V., 2003, MNRAS, 341, 1253
Hui L., Haiman Z., 2003, ApJ, 596, 9
Hurwitz M., Jenlinsky P., Dixon W. V., 1997, ApJ, 481, L31
Jang-Condell K., Hernquist L., 2001, ApJ, 548, 68
Kitayama T., Susa H., Umemura M., Ikeuchi S., 2001, MNRAS, 326, 1353
Kogut A. et al., 2003, ApJ, 148, 161
Leitherer C., Ferguson H. C., Heckman T. M., Lowenthal J. D., 1995, ApJ, 454, L19
Machacek M. E., Bryan G. L., Abel T., 2003, MNRAS, 338, 273
Machacek M. E., Bryan G. L., Abel T., 2001, ApJ, 548, 509
Mackey J., Bromm V., Hernquist L., 2003, ApJ, 586, 1
Oh S. P., 2001, ApJ, 569, 558
Oh S. P., Haiman Z., Rees M. J., 2001a, ApJ, 553, 73
Oh S. P., Nollett K. P., Madau P., Wasserburg G. J., 2001b, ApJ, 562, L1
Omukai K., 2000, ApJ, 534, 809
Omukai K., Nishi R., 1999, ApJ, 518, 64
Razoumov A. O., Norman M. L., Abel T., Scott D., 2002, ApJ, 572, 695
Ricotti M., Gnedin N. Y., Shull J. M., 2001, ApJ, 560, 580
Ricotti M., Gnedin N. Y., Shull J. M., 2002a, ApJ, 575, 49
Ricotti M., Gnedin N. Y., Shull J. M., 2002b, ApJ, 575, 33
Ricotti M., Shull J. M, 2000, ApJ, 542, 548
Salvaterra R., Ferrara A., Schneider R., 2003, preprint (astro-ph/0304074)
Schaerer D., 2002, A&A, 382, 28
Schneider R., Ferrara A., Natarajan P., Omukai K., 2002, ApJ, 571, 30
Sokasian A., Abel T., Hernquist L., Springel V., 2003, MNRAS, 344, 607(Paper I)
Sokasian A., Abel T., Hernquist, 2002, MNRAS, 332, 601
Sokasian A., Abel T., Hernquist, 2001, New Astron., 6, 359
Spergel D. N. et al., 2003, ApJ, 148, 195
Springel V., Hernquist L., 2003, MNRAS, 339, 312
Springel V., Hernquist L., 2002, MNRAS, 333, 649
Steidel C. C., Pettini M., Adelberger K. L., 2001, ApJ, 546, 665
Theuns T., Schaye J., Zaroubi S., Kim T., Tzanavaris P., Carswell B., 2002, ApJ, 567, L103
Tumlinson J., Giroux M. L., Shull M. J., 2001, ApJ, 550, L1
Tumlinson J., Shull J. M., 2000, ApJ, 528, L65

Venkatesan A., Tumlinson J., Shull M. J., 2003, ApJ, 584, 621
Whalen D., Abel T., Norman M. L., 2003, ApJ, submitted (astro-ph/0310283)
White R. L., Becker R. H., Fan X., Strauss M. A., 2003, ApJ, 126, 1
Wood K., Loeb A., 2000, ApJ, 545, 86
Wyithe J. S. B., Loeb A., 2003a, ApJ, 588, 69
Wyithe J. S. B., Loeb A., 2003b, ApJ, 586, 693
Yoshida N., Sokasian A., Hernquist L., Springel V., 2003a, ApJ, 598, 73
Yoshida N., Sokasian A., Hernquist L., Springel V., 2003b, ApJ, 591, 1
Yoshida N., Abel T., Hernquist L., Sugiyama N., 2003c, ApJ, 592, 645
Yoshida N., Sugiyama N., Hernquist L., 2003d, MNRAS, 344, 481
Yoshida N., Bromm V., Hernquist L., 2003e, ApJ, submitted (astro-ph/0310443)
Zaldarriaga M., Furlanetto S. R., Hernquist L., 2003, ApJ, submitted (astro-ph/0311514)

This paper has been typeset from a TEX/LATEX file prepared by the author.